

Non-perturbative macroscopic theory of interfaces with discontinuous dielectric constant

Y. M. Beltukov^{*} and A. V. Rodina[†]

Ioffe Institute, Russian Academy of Sciences, 194021 St. Petersburg, Russia

A. Alekseev[‡]

Department of Mathematics, University of Geneva, CH-1211 Genève 4, Switzerland

Al. L. Efros[§]

Naval Research Laboratory, Washington, DC 20375, USA

(Dated: May 23, 2025)

Abstract

Discontinuity of dielectric constants at the interface is a common feature of all nanostructures and semiconductor heterostructures. It gives rise to a divergence of the self-interaction potential acting on a charge near the interface, and it presents an obstruction to a perturbative description. In several limiting cases, this problem can be avoided by zeroing out the carrier wave function at the interface. In this paper, we developed a non-perturbative theory which gives a self-consistent description of carrier propagation through an interface with dielectric discontinuity. It is based on conservation of the current density propagating through the interface, and it is formulated in terms of general boundary conditions (GBC) for the wave function at the interface with a single phenomenological parameter W . For these GBC, we find exact solutions of the Schrödinger equation near the interface and the carrier energy spectrum including resonances. Using these results, we describe the photo effect at the semiconductor/vacuum interface and the electron energy spectrum in the interface quantum well, as well as the dependence of these two phenomena on the interface parameter W .

I. INTRODUCTION

The electronic, optical, and transport properties of nanostructures with various shapes and their ensembles are mainly controlled by spatial confinement and dielectric confinement effects. The description of spatial confinements in spherical nanocrystals started in the early 1990s using the effective mass approximation [1, 2], and now is a well-developed theoretical field. The multiband effective mass theory can take into account both a complex multiband structure and nonparabolicity of conduction and valence bands in III-V [3–6], II-VI [7] and perovskite nanostructures [8]. It is applicable not only in spherical nanocrystals, but also in nanowires and nanorods [9], and in nanoplatelets [10]. Effective mass calculations are supported by multiple first principles calculations that include DFT and empirical pseudo-potential calculations [11–15] of structures containing more than one million atoms.

One of the important tools in the effective mass theory is general boundary conditions (GBC) (see [16]) applied at interfaces between materials with different properties. In this

* yaroslav.beltukov@mail.ioffe.ru

† anna.rodina@mail.ioffe.ru

‡ Anton.Alekseev@unige.ch

§ alex.l.efros.civ@us.navy.mil

approach, the interface is characterized by a transfer matrix T which relates the values of the wave function and of its normal derivative on the two sides of the interface. The requirement for the probability current to be conserved across the interface is equivalent to the property of the Hamiltonian of the system being self-adjoint, and the evolution of the system being a unitary operator. These requirements force the transfer matrix T to be a real matrix (up to an irrelevant total phase factor). A detailed analysis of GBC for abrupt boundaries is given in [17–21].

In contrast to successes of the theory of the spatial confinement, a self-consistent theory of dielectric confinement is limited to several specific cases. The main stumbling block for a quantitative theoretical description of this phenomenon is taking into account the interaction of the electron with the surrounding dielectric medium. It renormalizes the Coulomb interaction between any two charges, and for each electron it induces an effective mirror charge across the boundary between materials with different dielectric constants. The interaction of the electron with its mirror charge is referred to as self-interaction, and it corresponds to a singular potential near the interface. In the case of a flat semiconductor-dielectric interface of two materials with dielectric constants ε_1 and ε_2 , the electric charge e at distance z from such the interface leads to its polarization which can be described by a mirror charge creating the potential [22]:

$$U_{\text{self}}(z) = \begin{cases} \frac{q_1}{z} & z < 0, \text{ semiconductor} \\ \frac{q_2}{z} & z > 0, \text{ vacuum or dielectric.} \end{cases} \quad (1)$$

Here q_1 and q_2 are the Coulomb constants given by

$$q_1 = -\frac{e^2}{4\varepsilon_1} \frac{\varepsilon_1 - \varepsilon_2}{\varepsilon_1 + \varepsilon_2}, \quad q_2 = -\frac{e^2}{4\varepsilon_2} \frac{\varepsilon_1 - \varepsilon_2}{\varepsilon_1 + \varepsilon_2}.$$

We will focus on the situation of $\varepsilon_1 > \varepsilon_2$ which is typical for semiconductor-vacuum and semiconductor-dielectric interfaces. In this case, q_1 and q_2 are negative and $|q_2| > |q_1|$. Consequently, the mirror force inside a semiconductor is always repulsive leading to the dielectric confinement of carriers in nanostructures.

One simple model featuring a discontinuity of the dielectric constant is the heterostructures shown in Fig. 1. In the absence of a dielectric discontinuity, it is represented by a V -height step-like potential — the band offset — which is shown by the dashed lines. The description of carrier scattering, reflection, and propagation on such step-like potential is a

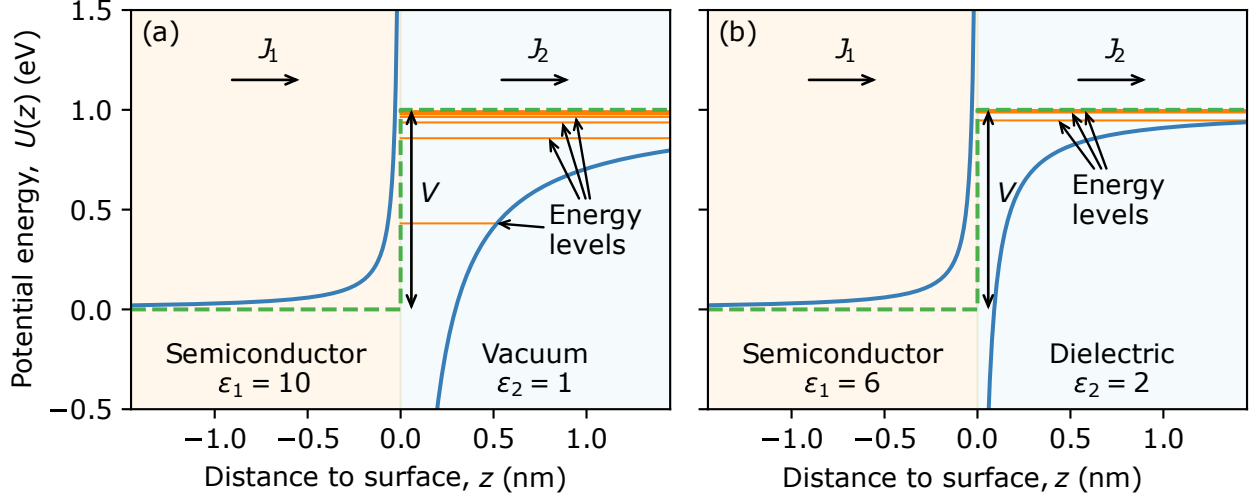


Figure 1. The heterostructure formed between the semiconductor and the vacuum (a) or the dielectric matrix (b). The dashed line shows the step-like potential due to the band offset $V = 1$ eV created by a semiconductor/vacuum (a) or by a semiconductor/dielectric matrix (b) interface. Solid lines show the sum of the step-like potential and the self-interacting potential, $U_{\text{self}}(z)$, created by mirror charge. The energy of the surface resonance levels (see Eq. (31)) created by the attractive potential $U_{\text{self}}(z)$ in the vacuum or in the dielectric are shown by horizontal orange lines.

standard textbook problem. At the same time, the mirror potential $U_{\text{self}}(z)$ described Eq.(1) gives rise to a $1/z$ divergence at $z = 0$.

The diverging mirror potential $U_{\text{self}}(z)$ cannot be consistently treated as a perturbation. Indeed, the first-order energy correction corresponding to $U_{\text{self}}(z)$ is given by the integral

$$\Delta E = \int |\psi(\mathbf{r})|^2 U_{\text{self}}(z) d^3\mathbf{r},$$

and this integral diverges at small z unless one imposes the condition that the wave function $\psi(\mathbf{r})$ vanishes at the interface $\psi(S) = 0$. The problem exists for all shapes of nanostructures because the mirror potential always has the same type of singularity at the nanostructure surface. In the multiband approximation, the problem does not disappear even if one imposes the condition $\psi_i(S) = 0$ on one of the components (*e.g.* the i -component) of the wave functions. In that case, the other components of the wave function will be proportional to the derivative $\psi'_i(z) \neq 0$ leading to divergences in the integrals [23]. A similar problem arises in calculations of surface-induced Rashba terms within the 14-band model [24].

Uncertainty in the carrier wave function magnitude at the interface created by $U_{\text{self}}(z)$

does not allow to describe its leakage into the matrix surrounding the nanostructures. This leakage is crucial for description of transport in nanocrystal arrays and solids [25, 26]. The absence of a coherent description of the leakage connected with mirror forces is even more critical for the quantitative description of the photo effect [27, 28].

Problems related to the singularity $U_{\text{self}} \sim 1/z$ have been addressed in the literature. Note that the $1/z$ divergence in $U_{\text{self}} \sim 1/z$ is unphysical [22] because one cannot use the microscopic potential at the inter-atomic distances to the interface. To mimic the *real* potential, one can introduce an intermediate region extending from $z = -d$ to $z = d$ (for some small d), and to have a smooth transitional potential in this region interpolating between the Coulomb like potentials on the two sides of the interface. This procedure was first suggested in [29, 30], and later it was used to calculate the exciton binding energy in a quantum well located near the semiconductor surface [31]. In a somewhat different approach, in order to avoid divergences in the mirror potential in a dielectric quantum well, Kumagai and Takagahara [32] suggested to shift them by a small distance δ away from the interface, and they had shown that the dependence of the exciton binding energy on δ is very weak. Yet another possible approach (see [33]) is to introduce a gradual change of the dielectric constant between the two materials on some small inter atomic distance d . Note however that all these approaches are *ad hoc*, and that their results depend on the particular model chosen to represent the interface.

In this paper, we consider general boundary conditions (GBC) at the interface based on the conservation of the probability current across the interface:

$$J_{1,2}(z) = -i \frac{\hbar}{2m_{1,2}} (\psi_{1,2}^* \psi'_{1,2} - \psi_{1,2} \psi_{1,2}^{\prime*}). \quad (2)$$

Here ψ_1 and ψ_2 are the wave functions, ψ'_1 and ψ'_2 are their z -derivatives and m_1 and m_2 are the effective masses of electrons on the two sides of the interface. The divergence of the potential $U_{\text{self}}(z)$ manifests in the fact that the derivatives $\psi'_{1,2}(z)$ logarithmically diverge at the interface. Following [34], we introduce the modified derivatives $\tilde{\psi}'_{1,2}$ (see the next section for details) which are regular at the interface, and which can be used in the expression for the probability current.

Conservation of the probability current across the interface gives rise to a 3-parameter family of GBC described by the modified transfer matrix \tilde{T} . We will focus on the particular 1-parameter family suggested in [35] which supplements the conservation of the probability

current by the condition of continuity of the wave function at the interface. These boundary conditions have the form

$$\psi_2(0) = \psi_1(0), \quad \frac{1}{m_2}\tilde{\psi}'_2(0) = \frac{1}{m_1}\tilde{\psi}'_1(0) + \tilde{t}_{21}\psi_1(0). \quad (3)$$

Here \tilde{t}_{21} is the only nontrivial coefficient in the (modified) transfer matrix defining the GBC. It is convenient to parametrize it in terms of the parameter W which has dimensions energy·length:

$$\tilde{t}_{21} = \frac{2W}{\hbar^2}. \quad (4)$$

In very rough terms, W can be thought of as the strength of an additional short-range potential $W\delta(z)$ at the interface.

We obtain an exact solution of the model presented in Fig. 1, and we apply the GBC (3) to study electron scattering in the energy range $E > V$, resonances and tunneling under the barrier for $V > E > 0$, and the localized surface states for $E < 0$. We observe a number of interesting new phenomena. For $E > V$, for some values of the parameters the perfect transmission (zero reflection) can occur. Surprisingly, this effect may even occur at $E = V$ while without a dielectric discontinuity the transmission coefficient vanishes at $E = V$. In the region $V > E > 0$ we encounter resonances in the reflection coefficient and tunneling of the wave function under the barrier near the resonance energies. In the region $E < 0$, the system may have discrete energy levels corresponding to quantum states localized near the interface.

As an application, we study the effect of the parameter W on semiconductor photo-ionization, and on electron confinement and wave function leakage in a quantum well at the semiconductor surface. Again, we encounter several new phenomena. It turns out that the photo-ionization may be enhanced by taking into account the influence of the mirror potential $U_{\text{self}}(z)$. For a quantum well, we observe a strong coupling between the quantum levels localized in the well and the surface states created by the attractive mirror potential.

The structure of the paper is as follows: in Section II, using the conservation of the current density we derive the general boundary conditions. In Section III, we find exact solutions for the carrier wave functions and their asymptotics for $z \rightarrow 0$ and for $z \rightarrow \pm\infty$. In Section IV, we study electron scattering at the interface in the energy range $E > V$, reflection and tunneling under the barrier for $V > E > 0$, and surface localized states for $E < 0$. We also introduce universal equations that describe scattering resonances and localized states.

In Section V, we apply our theory to describe efficiency of electron photoemission as well as the energy level structure in surface quantum well, and their dependence on the surface parameter W . In Section VI, we outline possible future applications of our theory.

II. BOUNDARY CONDITIONS FOR INTERFACES WITH DISCONTINUOUS DIELECTRIC CONSTANT

In this Section, we consider Hamiltonians of the form

$$\hat{H} = \begin{cases} -\frac{\hbar^2}{2m_1} \frac{d^2}{dz^2} + \frac{q_1}{z} + U_1^{\text{reg}}(z), & \text{for } z < 0, \\ -\frac{\hbar^2}{2m_2} \frac{d^2}{dz^2} + \frac{q_2}{z} + U_2^{\text{reg}}(z), & \text{for } z > 0. \end{cases} \quad (5)$$

Here the region $z < 0$ is a semiconductor, the region $z > 0$ is the vacuum or a dielectric, and the interface between the two materials is located at $z = 0$. The potentials $U_{1,2}^{\text{reg}}(z)$ are regular functions of z . Independently of the exact form of $U_{1,2}^{\text{reg}}(z)$, eigenfunctions of Hamiltonians (5) admit the following asymptotic behavior near $z = 0$:

$$\psi_{1,2}(z) = a_{1,2} + b_{1,2}z + c_{1,2}z \ln\left(\frac{|z|}{\lambda}\right) + d_{1,2}z^2 \ln\left(\frac{|z|}{\lambda}\right) + \dots \quad (6)$$

Here we denote by $\psi_1(z)$ the wave function for $z < 0$, and by $\psi_2(z)$ the wave function for $z > 0$. We have introduced the characteristic length λ which enters the logarithms. One can see that the magnitude of λ does not affect the logarithmic divergence of the wave functions at $z \rightarrow 0$ in Eq. (6). We will discuss possible choices of λ in the end of this Section.

Conditions

$$c_{1,2} = 2 \frac{m_{1,2}q_{1,2}}{\hbar^2} a_{1,2}, \quad d_{1,2} = 2 \left(\frac{m_{1,2}q_{1,2}}{\hbar^2} \right)^2 a_{1,2} \quad (7)$$

ensure that the function $\hat{H}\psi(z)$ has no singularity at $z = 0$. Using Eq. (6), we obtain the asymptotic behavior of derivatives of the wave function for $z < 0$ and for $z > 0$:

$$\psi'_{1,2}(z) = (b_{1,2} + c_{1,2}) + d_{1,2}z + c_{1,2} \ln\left(\frac{|z|}{\lambda}\right) + 2d_{1,2}z \ln\left(\frac{|z|}{\lambda}\right) + \dots, \quad (8)$$

and observe that they diverge at $z = 0$. This is the reason to introduce the modified derivatives

$$\tilde{\psi}'_{1,2}(z) = \psi'_{1,2}(z) - 2 \frac{m_{1,2}q_{1,2}}{\hbar^2} \psi_{1,2}(z) \ln\left(\frac{|z|}{\lambda}\right) \quad (9)$$

which have no singularities near $z = 0$. It is crucial that the probability current defined in Eq. (2) can be expressed using the modified derivatives:

$$J_{1,2}(z) \equiv -i \frac{\hbar}{2m_{1,2}} \left(\psi_{1,2}^*(z) \tilde{\psi}'_{1,2}(z) - \psi_{1,2}(z) \tilde{\psi}_{1,2}'^*(z) \right) \quad (10)$$

The continuity of this probability current across the interface gives rise to a 3-parameter family of self-adjoint GBCs:

$$\begin{pmatrix} \psi_2 \\ \tilde{\psi}'_2(z)/m_2 \end{pmatrix} = \tilde{T}_{21} \begin{pmatrix} \psi_1 \\ \tilde{\psi}'_1(z)/m_1 \end{pmatrix}, \text{ where } \det[\tilde{T}_{21}] = \tilde{t}_{11}\tilde{t}_{22} - \tilde{t}_{12}\tilde{t}_{21} = 1. \quad (11)$$

Here the matrix elements \tilde{t}_{ij} of the modified transfer matrix \tilde{T}_{21} are characteristic of the interface region. If the Coulomb constants $q_{1,2}$ vanish, the modified derivatives become ordinary derivatives, and the transfer matrix \tilde{T}_{21} defines the usual GBC at the interface. In the presence of $q_{1,2}$, we would like to connect the matrix elements of the phenomenological transfer matrix \tilde{T}_{21} with mirror force potential without necessarily going into microscopic calculations.

In order to address this question, Golovaty [35] introduced an interface layer of thickness $2d$ with the short-range potential

$$U^{\text{sing}}(z) = \frac{1}{d^2} U(z/d) + \frac{\ln(d/\lambda)}{d} Q(z/d) + \frac{1}{d} V(z/d) \quad (12)$$

singular in the limit $d \rightarrow 0$. The regular functions U , Q and V are defined on the segment from -1 to 1 , and in Eq. (12) they are scaled to the interface layer extending from $-d$ to d . These three terms in $U^{\text{sing}}(z)$ have a different scaling in the limit $d \rightarrow 0$. In this limit, one of the following two things happens: either the domain splits into two non-interacting parts for $z < 0$ and $z > 0$ with Dirichlet boundary conditions ($\psi_1(0) = 0$ and $\psi_2(0) = 0$), or one obtains boundary conditions of the form [35]

$$\psi_2(0) = \theta \psi_1(0), \quad \frac{\theta}{m_2} \tilde{\psi}'_2(0) = \frac{1}{m_1} \tilde{\psi}'_1(0) + \frac{2W}{\hbar^2} \psi_1(0) \quad (13)$$

which correspond to the transfer matrix

$$\tilde{T}_{21} = \begin{pmatrix} \theta & 0 \\ 2W/\hbar^2 \theta & 1/\theta \end{pmatrix}. \quad (14)$$

The mirror force potential in Eq. (1) grows as $z^{-1} \sim d^{-1}$ towards the interface layer. In comparison, the term $d^{-2}U(z/d) \sim d^{-2}$ grows much faster than the mirror force potential.

Assuming that the potential within the boundary layer interpolates between the two mirror force potentials for $z < -d$ and for $z > d$ we consider it unlikely that the term $d^{-2}U(z/d) \sim d^{-2}$ arises in the limit of $d \rightarrow 0$. Hence, we will focus our attention on the simplified model with $U = 0$.

In that case, one obtains the Dirichlet boundary conditions $\psi_1(0) = \psi_2(0) = 0$ unless the following condition is verified:

$$\frac{1}{d} \int_{-d}^d Q(z/d) dz = \int_{-1}^1 Q(y) dy = q_2 - q_1. \quad (15)$$

If the condition (15) is satisfied, in the limit $d \rightarrow 0$ one obtains the boundary conditions that preserve the continuity of the wave function at the interface:

$$\psi_2(0) = \psi_1(0), \quad \frac{1}{m_2} \tilde{\psi}'_2(0) = \frac{1}{m_1} \tilde{\psi}'_1(0) + \frac{2W}{\hbar^2} \psi_1(0). \quad (16)$$

Here $\theta = 1$, and the parameter

$$W = \frac{1}{d} \int_{-d}^d V(z/d) dz = \int_{-1}^1 V(y) dy \quad (17)$$

is the integral of the term $V(z/d)/d$ across the interface layer. In the limit $d \rightarrow 0$, it can be interpreted as the coefficient in front of the term $W\delta(z)$ in the short-range potential [35]. For matrix entries of the transfer matrix, we have $\tilde{t}_{11} = \tilde{t}_{11} = 1$, $\tilde{t}_{12} = 0$, and $\tilde{t}_{21} = 2W/\hbar^2$.

Finally, the term $\ln(d/\lambda) Q(z/d)/d$ also scales faster than the mirror charge potentials for $d \rightarrow 0$. Therefore, it is also unlikely that such a term naturally arises in a realistic interface. Hence, if we considered the limit $d \rightarrow 0$, all interfaces with $q_1 \neq q_2$ would violate the condition (15), and would have been impenetrable.

In practice, however, we consider small but finite values of d . This allows us to model the interface potential using the term

$$U^{\text{sing}}(z) = \frac{1}{d} V_0(z/d) \quad (18)$$

that scales in the same way as the mirror force potential. At finite d we can present $U^{\text{sing}}(z)$ as a sum of two terms, using

$$\frac{1}{d} V_0(z/d) = \frac{\ln(d/\lambda)}{d} Q(z/d) + \frac{1}{d} V(z/d),$$

where the function Q satisfies the condition (15). This yields the following relation between the integral of the potential across the interface and the parameter W in the boundary

conditions:

$$W_0 = \frac{1}{d} \int_{-d}^d V_0 \left(\frac{z}{d} \right) dz = (q_2 - q_1) \ln \left(\frac{d}{\lambda} \right) + W. \quad (19)$$

The parameter W_0 is the bare microscopic parameter of the interface, while the parameter W is the macroscopic characteristic of the interface which may possibly be observed. The relation between them is given by the mirror force renormalization (19).

Equation (19) and the boundary conditions (16) can be reproduced assuming the validity of the effective mass approximation in the transition layer and continuity of the wave function. The Hamiltonian takes the form

$$\hat{H}_{\text{layer}} = \begin{cases} -\frac{\hbar^2}{2m_1} \frac{d^2}{dz^2} + \frac{q_1}{z} + U_1^{\text{reg}}(z), & \text{for } z < -d, \\ -\frac{d}{dz} \frac{\hbar^2}{2m(z)} \frac{d}{dz} + \frac{\ln(d/\lambda)}{d} Q(z/d) + \frac{1}{d} V(z/d), & \text{for } |z| < d, \\ -\frac{\hbar^2}{2m_2} \frac{d^2}{dz^2} + \frac{q_2}{z} + U_2^{\text{reg}}(z), & \text{for } z > d, \end{cases} \quad (20)$$

where $m(z)$ interpolates between m_1 for $z < -d$ and m_2 for $z > d$, and the kinetic energy is symmetrized to ensure that the Hamiltonian is self-adjoint [36]. Taking the integral $\int_{-d}^d \hat{H}_{\text{layer}}(z) \psi(z) dz$ and neglecting variation of the wave function across the interface region, we compute

$$\frac{1}{m_2} \psi'_2(d) - \frac{1}{m_1} \psi'_1(-d) = \frac{2}{\hbar^2} \int_{-d}^d \left(\frac{1}{d} V_0 \left(\frac{z}{d} \right) - E \right) \psi(z) dz = \frac{2}{\hbar^2} W_0 \psi(0), \quad (21)$$

where we have neglected the small term $2dE$ in comparison to W_0 . Replacing the wave function derivatives in Eq. (21) by the modified derivatives from Eq. (9) we finally obtain

$$\frac{1}{m_2} \tilde{\psi}'_2(d) - \frac{1}{m_1} \tilde{\psi}'_1(-d) = \frac{2}{\hbar^2} \left[W_0 + (q_1 - q_2) \ln \left(\frac{d}{\lambda} \right) \right] \psi(0) = \frac{2}{\hbar^2} W \psi(0).$$

Due to convergence of the modified derivatives $\tilde{\psi}'_{1,2}(d) \rightarrow \tilde{\psi}'_{1,2}(0)$ when $d \rightarrow 0$ we arrive at the GBC defined in Eq. (13).

Eq. (19) also allows us to estimate the effect of dielectric constant differences on the surface parameter W . In more detail, the transition layer thickness $2d$ should be on the order of inter-atomic distances. The length scale parameter λ in $\ln(d/\lambda)$ that controls the electron behavior outside of the interface layer should naturally satisfy the condition $d < \lambda$. There are three characteristic lengths describing the electron motion near the interfaces. The first two of them are the radii $\lambda_{1,2} = \hbar^2/(m_{1,2}|q_{1,2}|)$ of electron localization in the image

potentials. For $U_1^{\text{reg}} = 0$, $U_2^{\text{reg}} = V$, the third characteristic length is the typical depth $\lambda_V = \sqrt{\hbar^2/2m_2V}$ of the electron tunneling under the barrier V created by the band offset between the two solids. The natural choice is $\lambda = \min(\lambda_1, \lambda_2, \lambda_V)$, the smallest of the three characteristic lengths. Note that the characteristic length λ is defined up to a numerical factor $\lambda \rightarrow \nu\lambda$. Such a rescaling results in the change of definitions of $\tilde{\psi}'_1$ and $\tilde{\psi}'_2$ (see Eq. (9)) and of the parameter W (see Eq. (19)), while all physical quantities remain the same. This redefinition can be interpreted as a finite renormalization in the framework of renormalization theory.

It is important that we apply boundary conditions to the effective mass wave functions at the interface ($z = 0$) where they are well defined. This allows us to use these wave functions for calculations of various physical characteristics within the effective mass approximation without any restrictions. At the same time, we do not know the microscopic details of the potential in the interface region and consider the surface parameter W as the phenomenological one.

III. EXACT SOLUTIONS

The Schrödinger equation for the Hamiltonian (5) admits exact solutions on both sides of the interface. For an arbitrary complex energy E , they are given by

$$\begin{aligned} \psi_1(z) &= ze^{\kappa_1 z} \left[C_1 M(1 + \alpha_1, 2, -2\kappa_1 z) + D_1 U(1 + \alpha_1, 2, -2\kappa_1 z) \right] \quad \text{for } z < 0 \\ \psi_2(z) &= ze^{-\kappa_2 z} \left[C_2 M(1 + \alpha_2, 2, 2\kappa_2 z) + D_2 U(1 + \alpha_2, 2, 2\kappa_2 z) \right] \quad \text{for } z > 0, \end{aligned} \quad (22)$$

where $M(a, b, z) = {}_1F_1(a, b, z)$ and $U(a, b, c)$ are the confluent hypergeometric functions of the first (Kummer's) and second (Tricomi's) kind, respectively. In Eq. (22) $\kappa_2 = \sqrt{2m_2(V - E)}/\hbar$ for the energies $E < V$ and $\kappa_1 = \sqrt{-2m_1 E}/\hbar$ for negative energies $E < 0$. For $E > 0$ we have $\kappa_1 = -ik_1$ with k_1 positive. Similarly, for $E > V$ we define $\kappa_2 = -ik_2$ with k_2 positive. In addition, it is convenient to introduce the following notation:

$$\alpha_1 = q_1 \kappa_1 / 2E, \quad \alpha_2 = q_2 \kappa_2 / 2(V - E). \quad (23)$$

For, $E > 0$ we denote $\alpha_1 = -i\beta_1$, and for $E > V$ we denote $\alpha_2 = -i\beta_2$ with β_1 and β_2 positive. The wave functions (22) should be accompanied by some boundary conditions at

the interface.

The asymptotics of the wave functions (22) for $z \rightarrow \pm\infty$ are given by:

$$\begin{aligned}\psi_1(z) &\simeq \frac{-1}{2\kappa_1} \left(\frac{C_1(-2\kappa_1 z)^{\alpha_1} e^{-\kappa_1 z}}{\Gamma(1+\alpha_1)} - \frac{C_1 e^{\kappa_1 z}}{(2\kappa_1 z)^{\alpha_1} \Gamma(1-\alpha_1)} + \frac{D_1 e^{\kappa_1 z}}{(-2\kappa_1 z)^{\alpha_1}} \right), \quad z \rightarrow -\infty, \\ \psi_2(z) &\simeq \frac{1}{2\kappa_2} \left(\frac{C_2(2\kappa_2 z)^{\alpha_2} e^{\kappa_2 z}}{\Gamma(1+\alpha_2)} - \frac{C_2 e^{-\kappa_2 z}}{(-2\kappa_2 z)^{\alpha_2} \Gamma(1-\alpha_2)} + \frac{D_2 e^{-\kappa_2 z}}{(2\kappa_2 z)^{\alpha_2}} \right), \quad z \rightarrow +\infty.\end{aligned}\quad (24)$$

The asymptotics of the wave functions (22) for $z \rightarrow 0$ are as follows:

$$\begin{aligned}\psi_1(z) &\simeq C_1 z + \frac{D_1}{\Gamma(\alpha_1)} \left(\frac{-1}{2\kappa_1 \alpha_1} + z \left[\ln(-2\kappa_1 z) - 1 + \sigma(\alpha_1) \right] \right), \quad z \rightarrow -0, \\ \psi_2(z) &\simeq C_2 z + \frac{D_2}{\Gamma(\alpha_2)} \left(\frac{1}{2\kappa_2 \alpha_2} + z \left[\ln(2\kappa_2 z) - 1 + \sigma(\alpha_2) \right] \right), \quad z \rightarrow +0.\end{aligned}\quad (25)$$

Here we introduce

$$\sigma(\alpha) = 2\gamma + \frac{\Gamma'(\alpha)}{\Gamma(\alpha)} + \frac{1}{2\alpha}, \quad (26)$$

where $\gamma \approx 0.577216$ is Euler's constant. The function $\sigma(\alpha)$ has the following properties:

$$\sigma(\alpha) - \sigma(-\alpha) = -\pi \cot(\pi\alpha), \quad \sigma(i\beta) - \sigma(-i\beta) = i\pi \coth(\pi\beta). \quad (27)$$

It has simple poles at non-negative integers:

$$\sigma(\alpha) \simeq -\frac{1}{2\alpha} \text{ for } \alpha \rightarrow 0, \quad \sigma(\alpha) \simeq -\frac{1}{\alpha+n} \text{ for } \alpha \rightarrow -n. \quad (28)$$

The imaginary and real parts of $\sigma(\alpha)$ are shown in Fig. 2 as a function of α .

Using Eqs. (9) and (25) one can calculate the modified derivatives at $z = 0$:

$$\begin{aligned}\tilde{\psi}'_1(0) &= C_1 + \frac{D_1}{\Gamma(\alpha_1)} \left(\ln(2\kappa_1 \lambda_1) + \sigma(\alpha_1) \right), \\ \tilde{\psi}'_2(0) &= C_2 + \frac{D_2}{\Gamma(\alpha_2)} \left(\ln(2\kappa_2 \lambda_2) + \sigma(\alpha_2) \right).\end{aligned}\quad (29)$$

Using boundary conditions defined in Eq. (16), we can find the energy spectra and the corresponding wave functions.

Let us start from the limit $W \rightarrow \pm\infty$ that we have briefly discussed in the previous section. The problem splits into two non-interacting parts corresponding to Dirichlet boundary condition: $\psi_1(0) = 0$ and $\psi_2(0) = 0$ and may give rise to isolated eigenvalues of the problem. These boundary conditions imply $J(0) = 0$, and there is no probability current through the interface $z = 0$. Using the asymptotic behavior described by Eq. (25) we obtain

$$\psi_1(0) = -\frac{D_1}{2\kappa_1 \alpha_1 \Gamma(\alpha_1)}, \quad \psi_2(0) = \frac{D_2}{2\kappa_2 \alpha_2 \Gamma(\alpha_2)}. \quad (30)$$

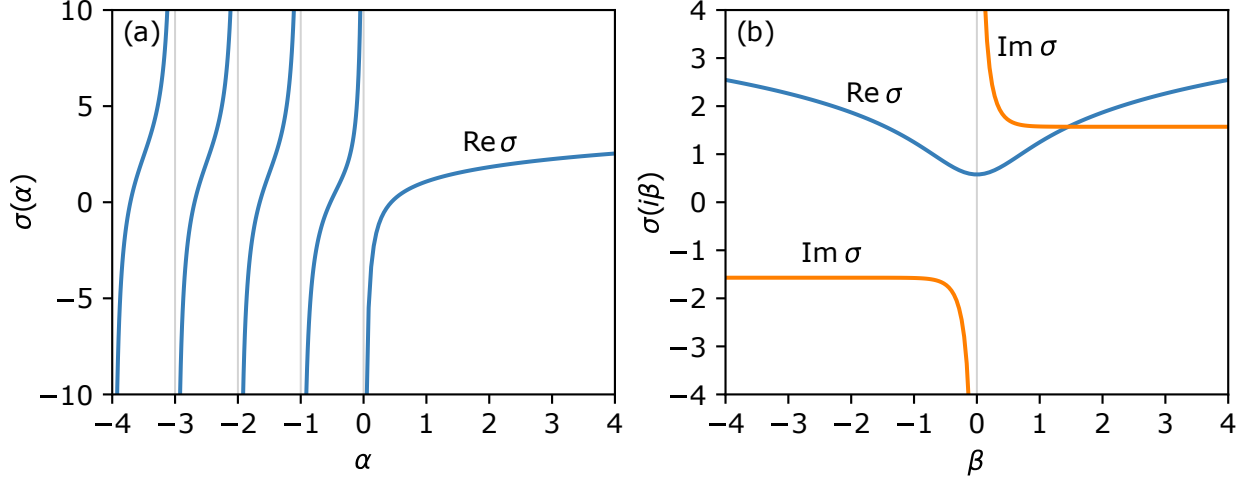


Figure 2. Function $\sigma(x)$ for (a) real ($x = \alpha$) and (b) imaginary ($x = i\beta$) arguments. Vertical gray lines show poles of $\sigma(x)$.

If $q_1, q_2 < 0$ the mirror force for $z > 0$ is attractive and leads to isolated eigenstates. The energy levels are connected with the poles of the Γ -function $\alpha_2 = -n$. The energy levels are given by:

$$E_n = V - \frac{\mathcal{R}_2}{n^2}, \quad \mathcal{R}_2 = \frac{m_2 q_2^2}{2\hbar^2} = \frac{\hbar^2}{2m_2 \lambda_2^2}. \quad (31)$$

We will refer to the energies E_n as the Dirichlet spectrum; the corresponding levels are shown in Fig. 1.

Now let us consider the solution at finite W . Imposing the boundary conditions described in Eq. (16) we obtain the relation between the coefficients $C_{1,2}$ and $D_{1,2}$:

$$D_1 = \left(\frac{C_1}{m_1} - \frac{C_2}{m_2} \right) \frac{m_1 q_1 \Gamma(\alpha_1)}{\Sigma(E) - W}, \quad D_2 = \left(\frac{C_1}{m_1} - \frac{C_2}{m_2} \right) \frac{m_2 q_2 \Gamma(\alpha_2)}{\Sigma(E) - W}, \quad (32)$$

where the complex function

$$\Sigma(E) = -q_1 (\ln(2\kappa_1 \lambda_1) + \sigma(\alpha_1)) + q_2 (\ln(2\kappa_2 \lambda_2) + \sigma(\alpha_2)) \quad (33)$$

is shown in Fig. 3. Function $\Sigma(E)$ plays a crucial role in the description of the energy spectra at the interface. In the energy region $E < 0$, Eq. (33) can be used directly since $\kappa_{1,2}$ are real positive and $\alpha_{1,2}$ are real. In the energy region $V > E > 0$, the expressions for $\Sigma(E)$ Eq. (33) is valid with $\kappa_1 = -ik_1$ and $\alpha_1 = -i\beta_1$ and can be rewritten as

$$\Sigma(E) = -q_1 \left(\ln(2k_1 \lambda_1) - \frac{i\pi}{2} + \sigma(-i\beta_1) \right) + q_2 (\ln(2\kappa_2 \lambda_2) + \sigma(\alpha_2)). \quad (34)$$

Finally, in the energy region $E > V$ we can rewrite $\Sigma(E)$ as

$$\Sigma(E) = -q_1 \left(\ln(2k_1\lambda_1) - \frac{i\pi}{2} + \sigma(-i\beta_1) \right) + q_2 \left(\ln(2k_2\lambda_2) - \frac{i\pi}{2} + \sigma(-i\beta_2) \right). \quad (35)$$

The imaginary part of $\Sigma(E)$ can be simplified using the identity $\text{Im } \sigma(-i\beta) = -(\pi/2) \coth(\pi\beta)$ for real β (which results from Eq. (27)). This yields:

$$\text{Im } \Sigma(E) = \begin{cases} G_1(E) + G_2(E), & E > V, \\ G_1(E), & 0 < E < V, \\ 0, & E < 0, \end{cases} \quad (36)$$

where

$$G_1(E) = \frac{\pi q_1}{1 - \exp(-2\pi\beta_1)} = \frac{\pi q_1}{1 - \exp\left(-\pi q_1 \sqrt{2m_1/E\hbar^2}\right)}, \quad (37)$$

$$G_2(E) = \frac{-\pi q_2}{1 - \exp(2\pi\beta_2)} = \frac{-\pi q_2}{1 - \exp\left(\pi q_2 \sqrt{2m_2/(E-V)\hbar^2}\right)}. \quad (38)$$

When the dielectric constants are equal to each other and $q_1, q_2 \rightarrow 0$, the function $\Sigma(E)$ tends to the function $\Sigma_0(E)$ given by

$$\Sigma_0(E) = \begin{cases} i\hbar\sqrt{\frac{E}{2m_1}} + i\hbar\sqrt{\frac{E-V}{2m_2}}, & E > V, \\ i\hbar\sqrt{\frac{E}{2m_1}} - \hbar\sqrt{\frac{V-E}{2m_2}}, & 0 < E < V, \\ -\hbar\sqrt{\frac{-E}{2m_1}} - \hbar\sqrt{\frac{V-E}{2m_2}}, & E < 0. \end{cases} \quad (39)$$

The functions $\Sigma(E)$ and $\Sigma_0(E)$ are shown in Fig. 3. One can see that $\Sigma(E)$ tends to $\Sigma_0(E)$ at high energy.

Note, that both $G_1(E)$ and $G_2(E)$ are positive because q_1 and β_1 have the same sign, while q_2 and β_2 have opposite signs, and $G_1(0) = \pi \max(q_1, 0)$, $G_2(V) = \pi \max(-q_2, 0)$. The finite value of $G_2(V) = -\pi q_2$ in the case $q_1, q_2 < 0$ is responsible for the jump of the $\text{Im } \Sigma(E)$ at $E = V$ while there is no jump at $E = 0$ (see in Fig. 3). This jump is vanishing with $q_2 \rightarrow 0$, and it is absent in $\text{Im } \Sigma_0(E)$.

IV. SCATTERING, RESONANCES, AND DISCRETE SPECTRUM

In this Section, we consider scattering, reflection, and propagation of electrons through interfaces separating two solids with different dielectric constants ($q_1 \neq 0$ and $q_2 \neq 0$) as

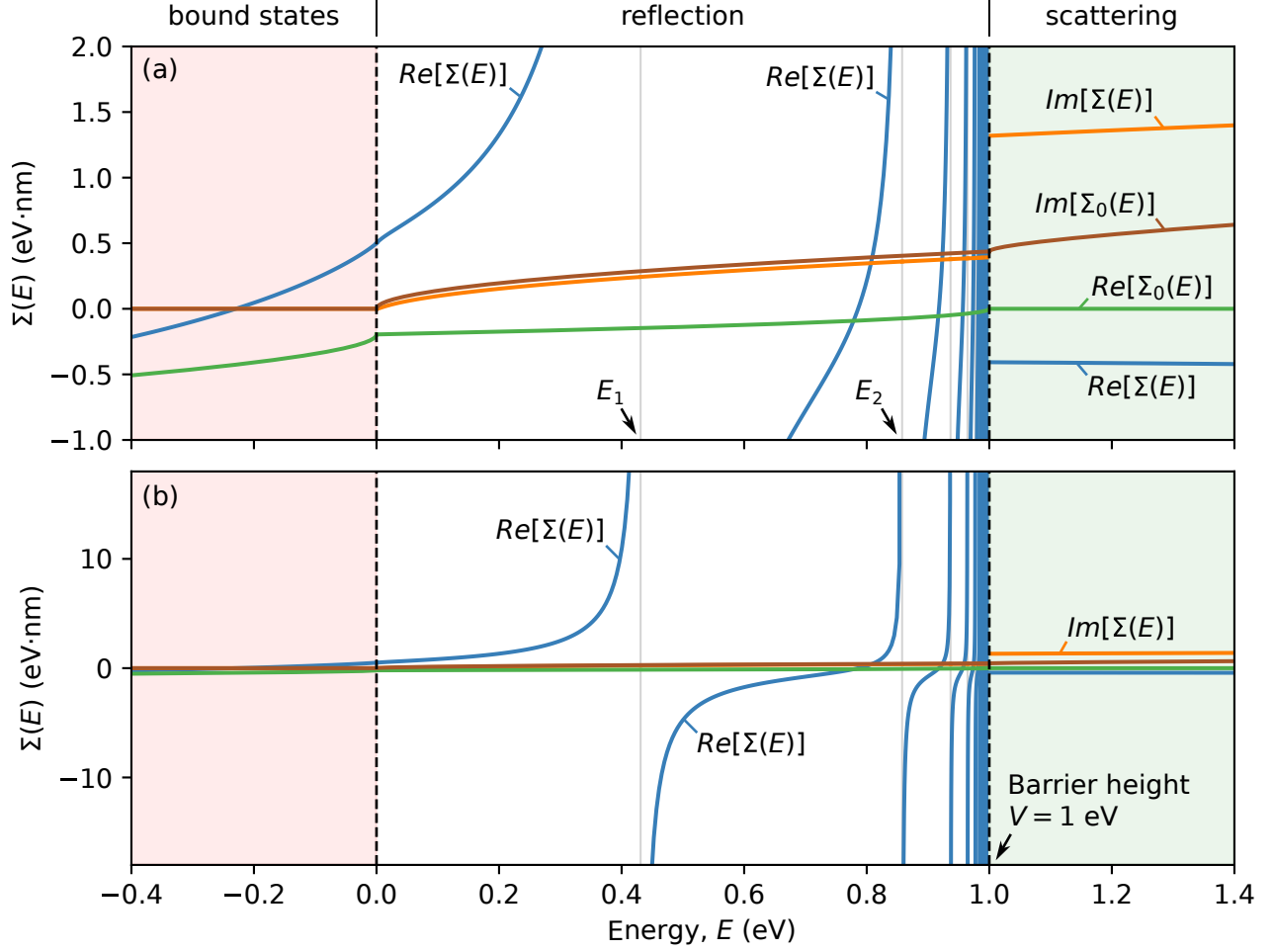


Figure 3. Dependence of $\Sigma(E)$ and $\Sigma_0(E)$ on the energy E , calculated for barrier height $V = 1$ eV. Vertical gray lines show poles $E = E_n$. Panels (a) and (b) differ in vertical scale only. The range $E < 0$ where the surface bound states might exist is marked by the rosa color; in the white region $0 < E < V$ the under barrier reflection takes place; in the green region $E > V$ the scattering and reflection above the barrier occurs.

shown in Fig. 1. We have a separate discussion for each of the three energy regions: $E > V$, $V > E > 0$ and $E < 0$.

A. Reflection and propagation for $E > V$

We first consider the scattering problem for $E > V > 0$. The asymptotics of the wave functions for $z \rightarrow \pm\infty$ can be written as:

$$\begin{aligned}\psi_1(z) &\simeq A_1 e^{ik_1 z - i\beta_1 \ln(-2k_1 z)} + B_1 e^{-ik_1 z + i\beta_1 \ln(-2k_1 z)}, \\ \psi_2(z) &\simeq A_2 e^{ik_2 z + i\beta_2 \ln(2k_2 z)} + B_2 e^{-ik_2 z - i\beta_2 \ln(2k_2 z)}.\end{aligned}\quad (40)$$

Note that the plane wave asymptotic behavior in Eq. (40) has long-range logarithmic corrections from the Coulomb potential. The coefficients $A_{1,2}, B_{1,2}$ in Eq. (40) are related to coefficients $C_{1,2}, D_{1,2}$ from Eq. (24) as follows:

$$\begin{aligned}A_1 &= -\frac{iC_1}{2k_1} \frac{e^{-\pi\beta_1/2}}{\Gamma(1-i\beta_1)}, & B_1 &= \frac{iC_1}{2k_1} \frac{e^{-\pi\beta_1/2}}{\Gamma(1+i\beta_1)} - \frac{iD_1}{2k_1} e^{\pi\beta_1/2}, \\ A_2 &= -\frac{iC_2}{2k_2} \frac{e^{-\pi\beta_2/2}}{\Gamma(1+i\beta_2)} + \frac{iD_2}{2k_2} e^{\pi\beta_2/2}, & B_2 &= \frac{iC_2}{2k_2} \frac{e^{-\pi\beta_2/2}}{\Gamma(1-i\beta_2)}.\end{aligned}\quad (41)$$

Using Eq. (32), we can express four coefficients $A_{1,2}, B_{1,2}$ in terms $C_{1,2}$. For arbitrary $C_{1,2}$ the relationships between $A_{1,2}, B_{1,2}$ can be written with the help of the scattering matrix $S(W, E)$:

$$\begin{pmatrix} B_1 \\ A_2 \end{pmatrix} = S(W, E) \begin{pmatrix} A_1 \\ B_2 \end{pmatrix}, \quad (42)$$

where

$$S(W, E) = \begin{pmatrix} \frac{\Gamma(-i\beta_1)}{\Gamma(i\beta_1)} - \frac{iq_1\beta_1\Gamma^2(-i\beta_1)}{\Sigma(E)-W} e^{\pi\beta_1} & \frac{iq_2\beta_1\Gamma(-i\beta_1)\Gamma(-i\beta_2)}{\Sigma(E)-W} e^{\frac{\pi}{2}(\beta_1+\beta_2)} \\ -\frac{iq_1\beta_2\Gamma(-i\beta_1)\Gamma(-i\beta_2)}{\Sigma(E)-W} e^{\frac{\pi}{2}(\beta_1+\beta_2)} & \frac{\Gamma(-i\beta_2)}{\Gamma(i\beta_2)} + \frac{iq_2\beta_2\Gamma^2(-i\beta_2)}{\Sigma(E)-W} e^{\pi\beta_2} \end{pmatrix}. \quad (43)$$

For $q_{1,2} \rightarrow 0$, the scattering matrix $S(W, E)$ tends to the limit $S_0(W, E)$ which describes scattering on the step-like barrier (without Coulomb potential):

$$S_0(W, E) = \frac{1}{\Sigma_0(E) - W} \begin{pmatrix} i\frac{\hbar^2}{2} \left(\frac{k_1}{m_1} - \frac{k_2}{m_2} \right) + W & i\hbar^2 \frac{k_2}{m_2} \\ i\hbar^2 \frac{k_1}{m_1} & i\frac{\hbar^2}{2} \left(\frac{k_2}{m_2} - \frac{k_1}{m_1} \right) + W \end{pmatrix} \quad (44)$$

For $E > V$, the scattering matrix $S(W, E)$ satisfies the unitary condition:

$$S(W, E)^* K S(W, E) = K, \quad K = \begin{pmatrix} k_1/m_1 & 0 \\ 0 & k_2/m_2 \end{pmatrix}. \quad (45)$$

This condition follows from the conservation of the probability current on the two sides of the interface.

The reflection coefficient R and the transmission coefficient $T_{\text{tr}} = 1 - R$ (defined as electron fluxes normalized to the incident flux [27]) can be expressed via the elements of the scattering matrix:

$$R(W, E) = |S_{11}(W, E)|^2 = |S_{22}(W, E)|^2, \quad T_{\text{tr}}(W, E) = |S_{12}(W, E)S_{21}(W, E)|. \quad (46)$$

Substituting the expressions for these matrix elements from Eq. (43) we obtain the reflection coefficient

$$R(W, E) = 1 - \frac{4G_1(E)G_2(E)}{|\Sigma(E) - W|^2} = \frac{(\text{Re } \Sigma(E) - W)^2 + (G_1(E) - G_2(E))^2}{(\text{Re } \Sigma(E) - W)^2 + (G_1(E) + G_2(E))^2}, \quad (47)$$

and the transmission coefficient

$$T_{\text{tr}}(W, E) = 1 - R(W, E) = \frac{4G_1(E)G_2(E)}{|\Sigma(E) - W|^2}. \quad (48)$$

For complex values of E , the scattering matrix $S(W, E)$ has poles corresponding to resonances at solutions of the equation $\Sigma(E) = W$. However, for $\text{Re } E > V$ the imaginary part $\text{Im } \Sigma(E) = G_1(E) + G_2(E)$ is always positive and does not vanish even for complex energies E . One can observe maxima of the transmission coefficient (and minima of the reflection coefficient) near solutions of the equation $\text{Re } \Sigma(E) = W$.

In what follows, we discuss an interesting phenomenon of perfect transmission ($T_{\text{tr}} = 1$) which may occur due to dielectric confinement.

Perfect transmission (that is, zero reflection) occurs at the energies E_{tr} and boundary condition parameters W_{tr} that simultaneously satisfy the equations $G_1(E_{\text{tr}}) = G_2(E_{\text{tr}})$ and $\text{Re } \Sigma(E_{\text{tr}}) = W_{\text{tr}}$. The graphs of functions $G_1(E)$ and $G_2(E)$ intersecting at $E = E_{\text{tr}}$ are shown in Fig. 4(a). The corresponding value of W_{tr} can be seen in Fig. 4(b). The dependence of E_{tr} and W_{tr} on the dielectric constant ε_1 at the semiconductor/vacuum interface ($\varepsilon_2 = 1$) is shown in Fig. 4(c,d).

Surprisingly, perfect transmission may occur exactly at $E_{\text{tr}} = V$. For given values of the parameters $\varepsilon_1, \varepsilon_2, m_1, m_2$, the perfect transmission at $E_{\text{tr}} = V$ takes place for $V = V_{\text{tr}}$ given by the following formula

$$V_{\text{tr}} = \frac{4\pi^2 \mathcal{R}_1}{\ln^2(1 + \varepsilon_2/\varepsilon_1)}, \quad \mathcal{R}_1 = \frac{m_1 q_1^2}{2\hbar^2} = \frac{\hbar^2}{2m_1 \lambda_1^2}. \quad (49)$$

For comparison, for $\varepsilon_1 = \varepsilon_2$ and $q_{1,2} = 0$, the transmission coefficient can be written as

$$T_0(W, E) = \frac{2\hbar^2 \sqrt{E(E - V)}}{\sqrt{m_1 m_2} |\Sigma_0(E) - W|^2}. \quad (50)$$

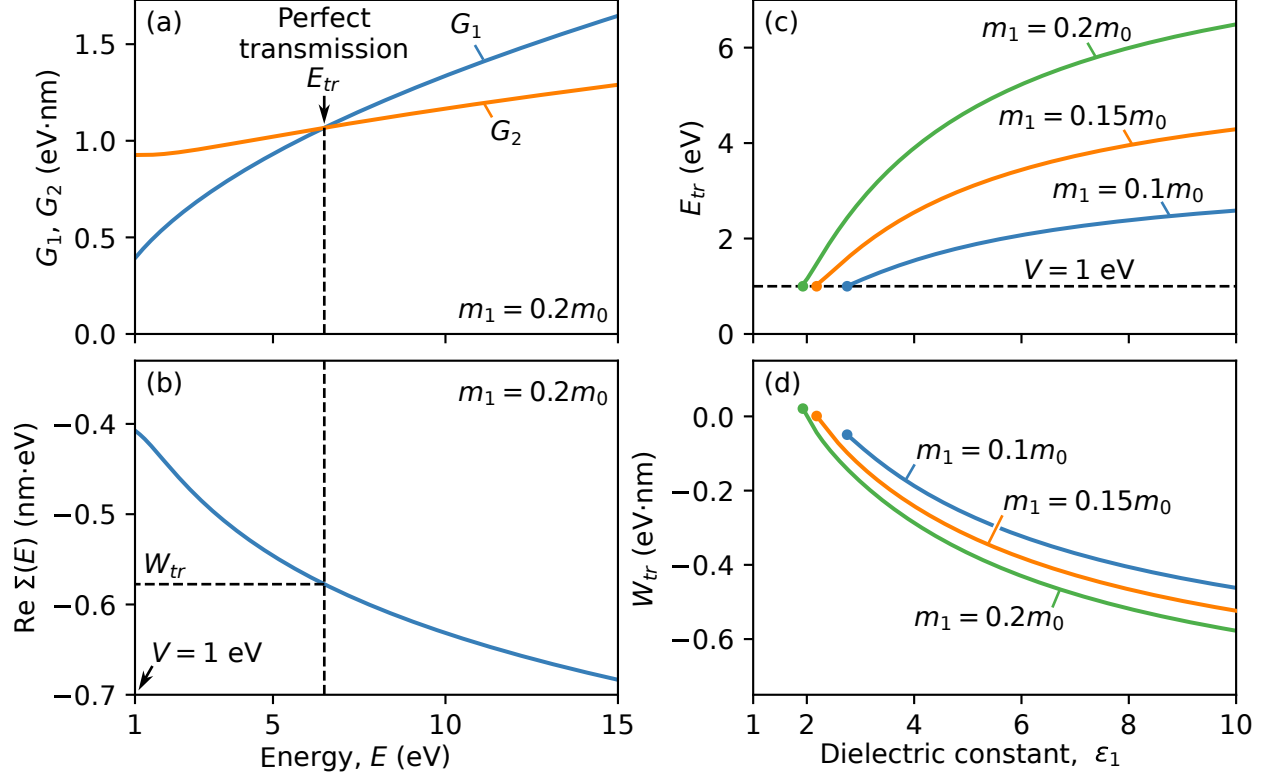


Figure 4. (a, b). Calculation of the perfect transmission energy $E_{tr} > V$ and surface parameter W_{tr} in structures with dielectric constants $\epsilon_2 = 1$ and $\epsilon_1 = 10$, and electron effective masses $m_2 = m_0$, $m_1 = 0.2m_0$. (c, d) Dependencies of E_{tr} and W_{tr} on ϵ_1 for $\epsilon_2 = 1$, $m_2 = m_0$ and different values of m_1 . All calculations are conducted for the barrier height $V = 1$ eV.

The dependence of $T_0(0, E)$ on electron masses $m_1 \neq m_2$ and on the barrier height V was studied in Refs. [27, 28]. We note that $T_0(W, V) = 0$ while $T_{tr}(W, V)$ is non-vanishing even for small values of $q_1, q_2 \neq 0$.

For $W = 0$, several values of ϵ_1 , and $V = 1$ eV and $V = 0.2$ eV, the dependence of the transmission coefficient on the energy $E > V$ is shown in Fig. 5(a) and Fig. 5(c), respectively. One can see that for $\epsilon_1 = 1$ we have $T_0(0, V) = 0$ while $T_{tr}(0, V) \neq 0$ even for the values of ϵ_1 very close to one. In addition, $T_{tr}(0, E)$ changes non-monotonically with ϵ_1 due to the existence of perfect transmission points. Indeed, for ϵ_1 such that the condition $V \approx V_{tr}$ is verified (see Eq. (49)), the value of $T_{tr} \approx 1$ is nearly constant in the range of energies $V < E < V + k_B T$ which is painted over by the green color in Fig. 5(a) and Fig. 5(c). The dependence of V_{tr} on $E - V$ is shown by red and green lines in Fig. 5(a) and Fig. 5(c) at $T = 300$ K. For other values of ϵ_1 , T_{tr} is usually growing with E in this energy range.

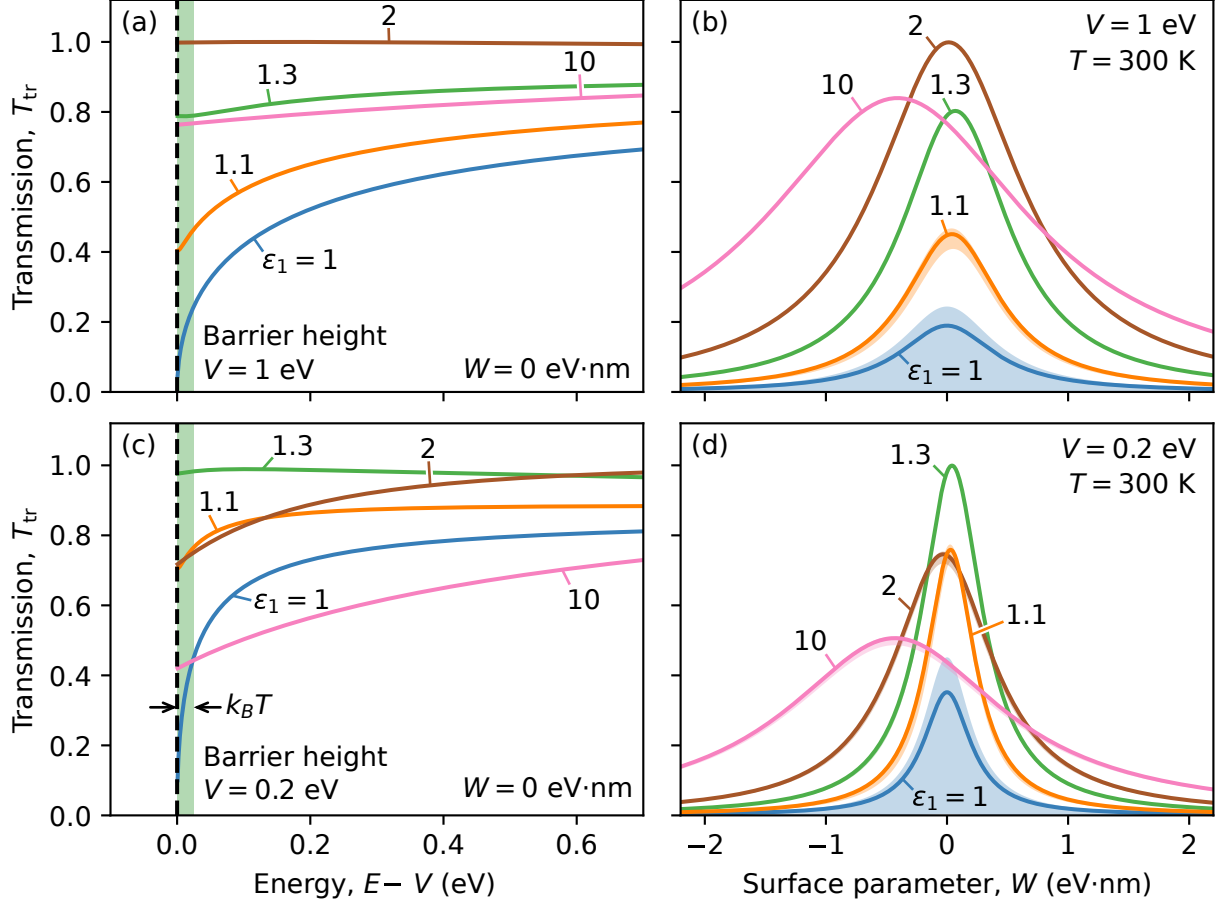


Figure 5. (a, c) Dependence of the transmission coefficient T_{tr} on energy $E - V$ for the surface parameter $W = 0$. (b, d) Dependence of the averaged transmission efficiency $T_{\text{tr}}^{\text{eff}}$ on the surface parameter W . In (a, c) the filled area shows the energy interval $V < E < V + k_B T$ with $T = 300$ K. The fill up the area in the (b) and (d) panels shows the room temperature distribution of the transmission coefficient T_{tr} in the same energy interval. The calculations are conducted for barrier height $V = 1$ eV (a, b) and $V = 0.2$ eV (c, d) and several dielectric constants ϵ_1 and $\epsilon_2 = 1$.

To analyze the impact of the dielectric confinement on the electron transmission, we plot the averaged transmission efficiency, $T_{\text{tr}}^{\text{eff}}$, representing the transmission coefficient averaged with the Boltzmann distribution of the electron energies $E > V$ (see Eq. (58) in the next Section) as a function of the surface parameter W , several values of ϵ_1 , and $V = 1$ eV and $V = 0.2$ eV, in Figures 5(b) and 5(d). They show rapid decrease of $T_{\text{tr}}^{\text{eff}}$ with increase of $|W|$. One can also see that $T_{\text{tr}}^{\text{eff}}$ reaches its maximum value at some value of the surface parameter $W_{\text{tr}} \neq 0$. Filled areas in Figs. 5(b) and 5(d) show T_{tr} in the energy range $V < E < V + k_B T$. The distribution of the transmission coefficient, however, is not observable for the values of

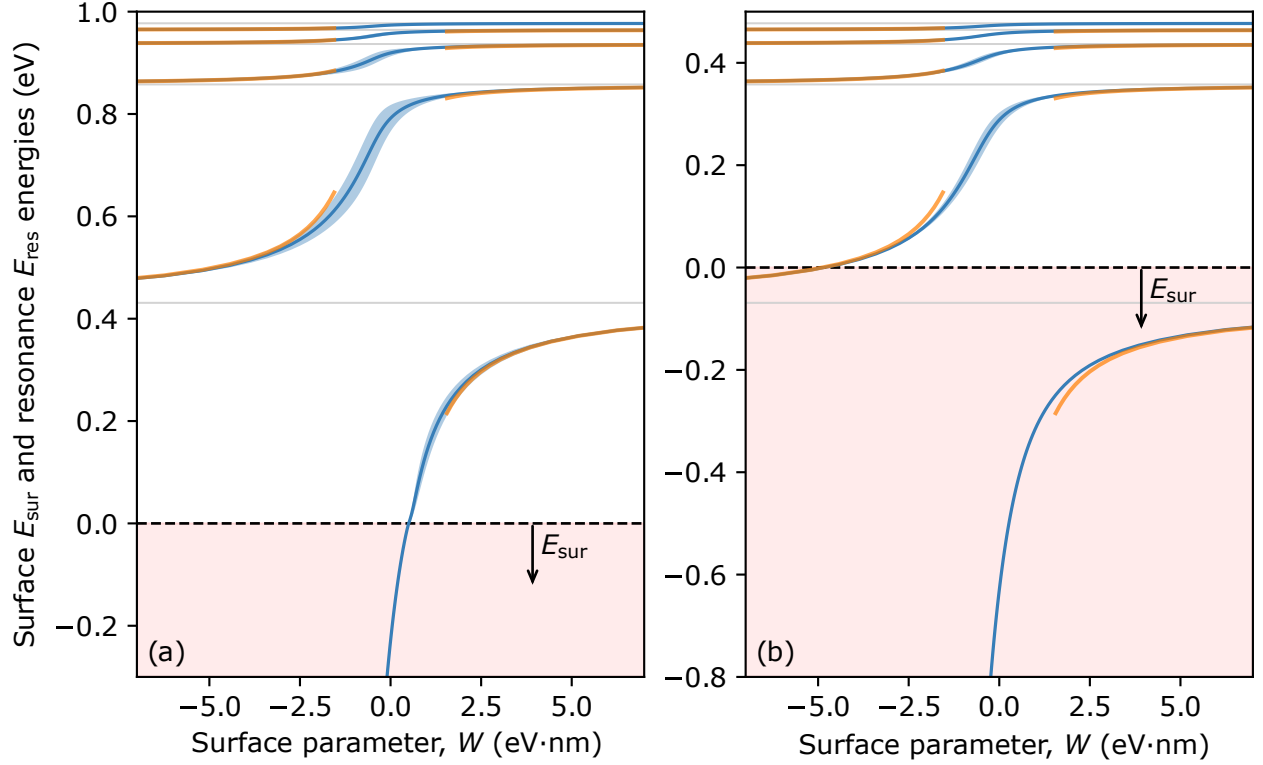


Figure 6. Dependence of resonance energies on the surface parameter W calculated for $V = 1$ eV (a) and for $V = 0.5$ eV (b). Imaginary part of E_{res} is shown by the thickness of the blue line. Horizontal lines show the asymptotic resonance energies E_n . The energies $E_{\text{sur}} < 0$ below the dashed line correspond to the surface localized states. Orange lines show the resonance energies calculated using asymptotic expression of Eq. (55) for $E_n^{\text{res}} > 0$ and of Eq. (56) for $E_n^{\text{sur}} < 0$.

ε_1 close to the “optimal”, due to nearly constant value of $T_{\text{tr}} \approx T_{\text{tr}}^{\text{eff}}$ in this energy range.

The zero reflection condition, $R_0(W, E_{\text{tr}}) = 1 - T_0(W, E_{\text{tr}}) = 0$, could also take place when $k_1(E_{\text{tr}})/m_1 = k_2(E_{\text{tr}})/m_2$ and $W = 0$, which means $E_{\text{tr}}/m_1 = (E_{\text{tr}} - V)/m_2$. One can see, that this equality cannot be realized for $m_1 < m_2$ and $V > 0$. Thus, the appearance of zero reflection and perfect transmission at some energies $E_{\text{tr}} \geq V$ as well as the nonzero transmission at $E = V$ are new properties brought by reflection from the image potential U_{self} .

B. Reflection and tunneling under the barrier for $V > E > 0$

Next, we consider the energy range $V > E > 0$. In this range, the wave function $\psi_2(z)$ decays for $z \rightarrow +\infty$, and the coefficient C_2 vanishes. Then, the reflection coefficient is equal

to one ($R = 1$), and the transmission coefficient vanishes ($T_{\text{tr}} = 0$).

The ratio $r(W, E)$ of the amplitudes of reflected and falling waves can be written as:

$$r(W, E) = \frac{B_1}{A_1} = \frac{\Gamma(-i\beta_1)}{\Gamma(i\beta_1)} \left(1 - \frac{2iG_1(E)}{\Sigma(E) - W} \right). \quad (51)$$

For real values of the energy in the range $V > E > 0$, $\text{Im} \Sigma(E) = G_1(E)$, and $r(W, E)$ can be rewritten as

$$r(W, E) = \frac{\Gamma(-i\beta_1) \Sigma^*(E) - W}{\Gamma(i\beta_1) \Sigma(E) - W} = e^{i\phi} \quad (52)$$

with the reflection phase ϕ given by

$$\phi = -2 \arg \Gamma(i\beta_1) - 2 \arctan \left(\frac{G_1(E)}{\text{Re} \Sigma(E) - W} \right). \quad (53)$$

Complex solutions of the equation $\Sigma(E) = W$ denoted by E_{res} correspond to resonances of the system. The dependence of $\text{Re} \Sigma(E)$ on energy E is shown in Fig. 3, and the dependence of $\text{Re} E_{\text{res}}$ on the parameter W is shown in Figs. 6(a) and 6(b) for $V = 1$ eV and $V = 0.5$ eV, respectively. The imaginary part $\text{Im} E_{\text{res}}$ is negative, and the value of $|\text{Im} E_{\text{res}}|$ gives the width of the resonance shown by the thickness of lines in Figs. 6.

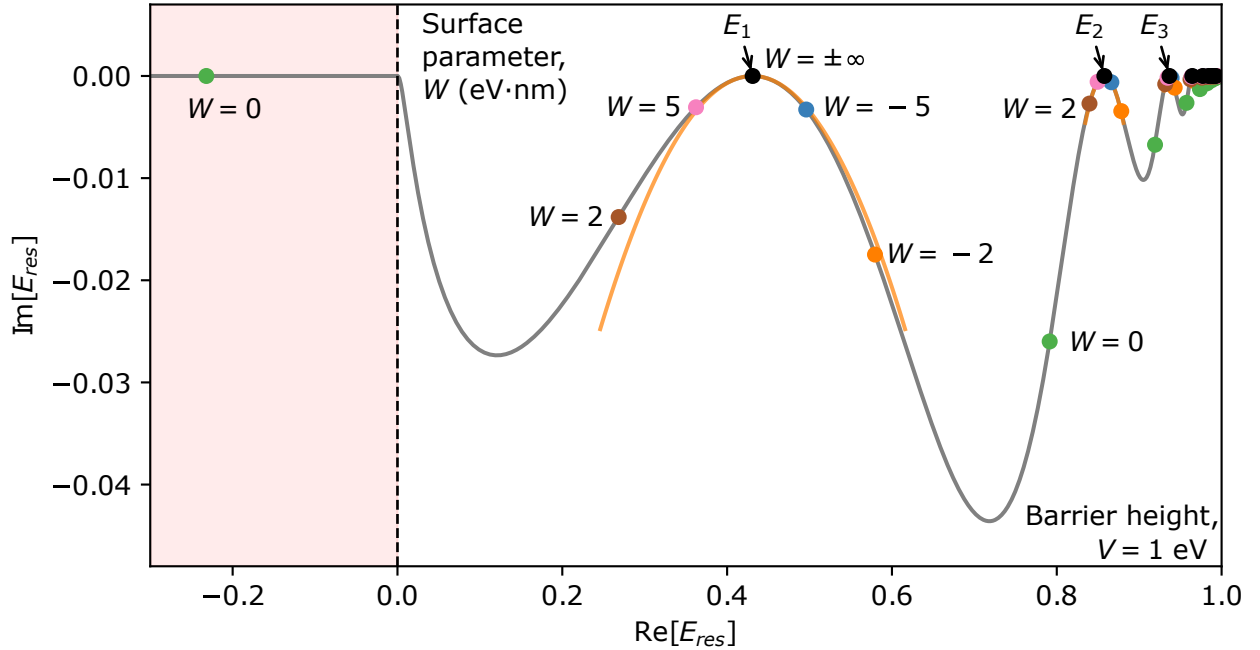


Figure 7. Resonance energies on the complex plane for different values of the surface parameter W , and for $V = 1$ eV. Orange lines represent the asymptotic formula (55).

For $W \rightarrow \pm\infty$, one can find the asymptotic expressions for the resonance energies E_n^{res} which are close to the Dirichlet energies E_n . In more detail, since $\sigma(\alpha_2)$ has poles at $E = E_n$

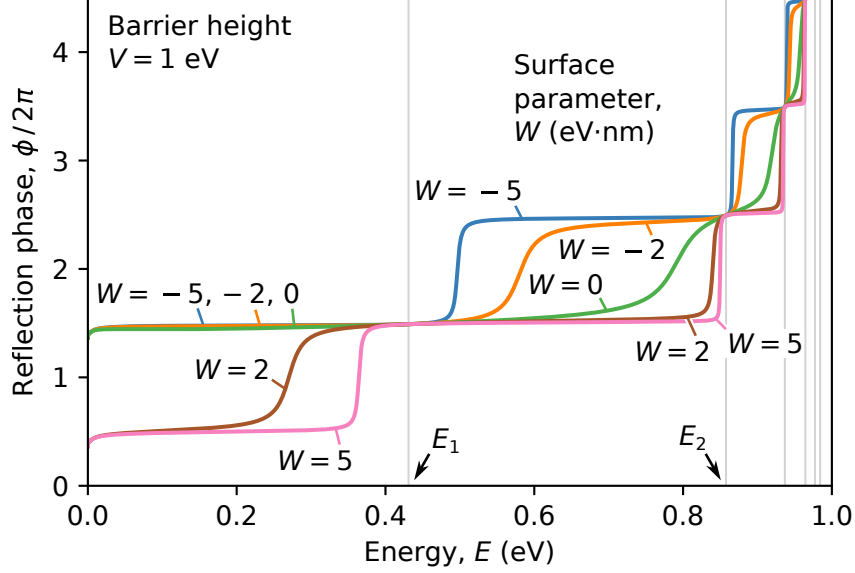


Figure 8. Dependence of the angle ϕ on the energy E calculated for $V = 1$ eV and for different values of the surface parameter W . Vertical gray lines show poles $E = E_n$.

(see Eq. (31)), so does the function $\Sigma(E)$. Near these poles, and for large values of $|W|$, the function $\Sigma(E)$ can be approximated as follows:

$$\Sigma(E) \simeq \frac{2q_2\mathcal{R}_2}{n^3(E - E_n)} + iG_1(E_n), \quad E \rightarrow E_n. \quad (54)$$

Assuming that the resonance energy E_n^{res} is close to E_n , one can approximate them as

$$E_n^{\text{res}} \simeq E_n + \frac{2q_2\mathcal{R}_2}{n^3(W - iG_1(E_n))} \simeq E_n + \frac{2q_2\mathcal{R}_2}{n^3W} + i\frac{2q_2\mathcal{R}_2G_1(E_n)}{n^3W^2}. \quad (55)$$

One can see from Eq. (55) that for $|W| \rightarrow \infty$, the resonance energy E_n^{res} tends to E_n along a parabola (see Fig. 7). This is a characteristic behavior of resonances tending to points of the discrete spectrum. Note again that $\text{Im } E_n^{\text{res}} < 0$, and that the quantity $|\text{Im } E_n^{\text{res}}| = |2q_2\mathcal{R}_2G_1/(n^3W^2)|$ is the width of the n 'th resonance.

For several values of W , the dependence of the reflection phase angle ϕ on the electron energy is shown in Fig. 8. Note that the phase ϕ experiences jumps of 2π near resonances.

C. Surface states below the semiconductor band edge

Surface states can be created by the attractive mirror force potential below the semiconductor band edge $E = 0$. The condition for the wave function to decay for $z \rightarrow \pm\infty$ on both

sides of the interface yields $C_1 = C_2 = 0$. We start with the analysis of Dirichlet boundary conditions $\psi_1(0) = \psi_2(0)$ which correspond to the limit $|W| \rightarrow \infty$. In that case, the isolated eigenvalues arise for $z > 0$, and they correspond to the poles of the function $\Gamma(\alpha_2)$ at the points $\alpha_2 = -n$, and to the Dirichlet energies E_n given by Eq. (31).

For finite values of W , the discrete spectrum is again given by solutions of the equation $\Sigma(E) = W$. The behavior of the function $\Sigma(E)$ for $E < 0$ is shown in Fig. 3. In the energy range $E < 0$, solutions of the equation $\Sigma(E) = W$ denoted by E_{sur} are shown in Fig. 6.

In the case of $\mathcal{R}_2 > V$, some of the Dirichlet energies E_n might be negative (Fig. 6(b)). They correspond to the poles of the function $\sigma(\alpha_2)$ for negative integer values of α_2 . At the same time, the values of α_1 are positive and the function $\sigma(\alpha_1)$ does not have poles. Using the same asymptotic analysis as in the previous section, we obtain the following asymptotics valid for large values of $|W|$:

$$E_n^{\text{sur}} \approx E_n + \frac{2\mathcal{R}_2}{n^3} \frac{q_2}{W}. \quad (56)$$

This formula can be compared to Eq. (55), where $G_1(E) = 0$ for $E < 0$.

V. APPLICATIONS: PHOTOEMISSION AND SURFACE QUANTUM WELL

In this Section, we consider two applications of our approach to heterostructures of the type shown in Fig. 1. The first concerns the photoemission of electrons from the semiconductor to vacuum, and the second is the study of quantum states confined in a quantum well located near the surface of a semiconductor. While the discontinuity of the self-interaction potential affects multiple phenomena in optical and electrical properties of nanostructures, we selected these two effects because they can be described within the one-dimensional model developed above.

A. Electron photoemission

First, we address the influence of the dielectric discontinuity on photoemission. In our model, we neglect a semiconductor doping which leads to band bending near the semiconductor/vacuum interface and to acceleration of electrons falling on the surface (see Fig. 1 [28]). Consequently, only electrons with kinetic energy larger than band offset V contribute to the photoemission. The quantum efficiency Y of electron photoemission is defined in

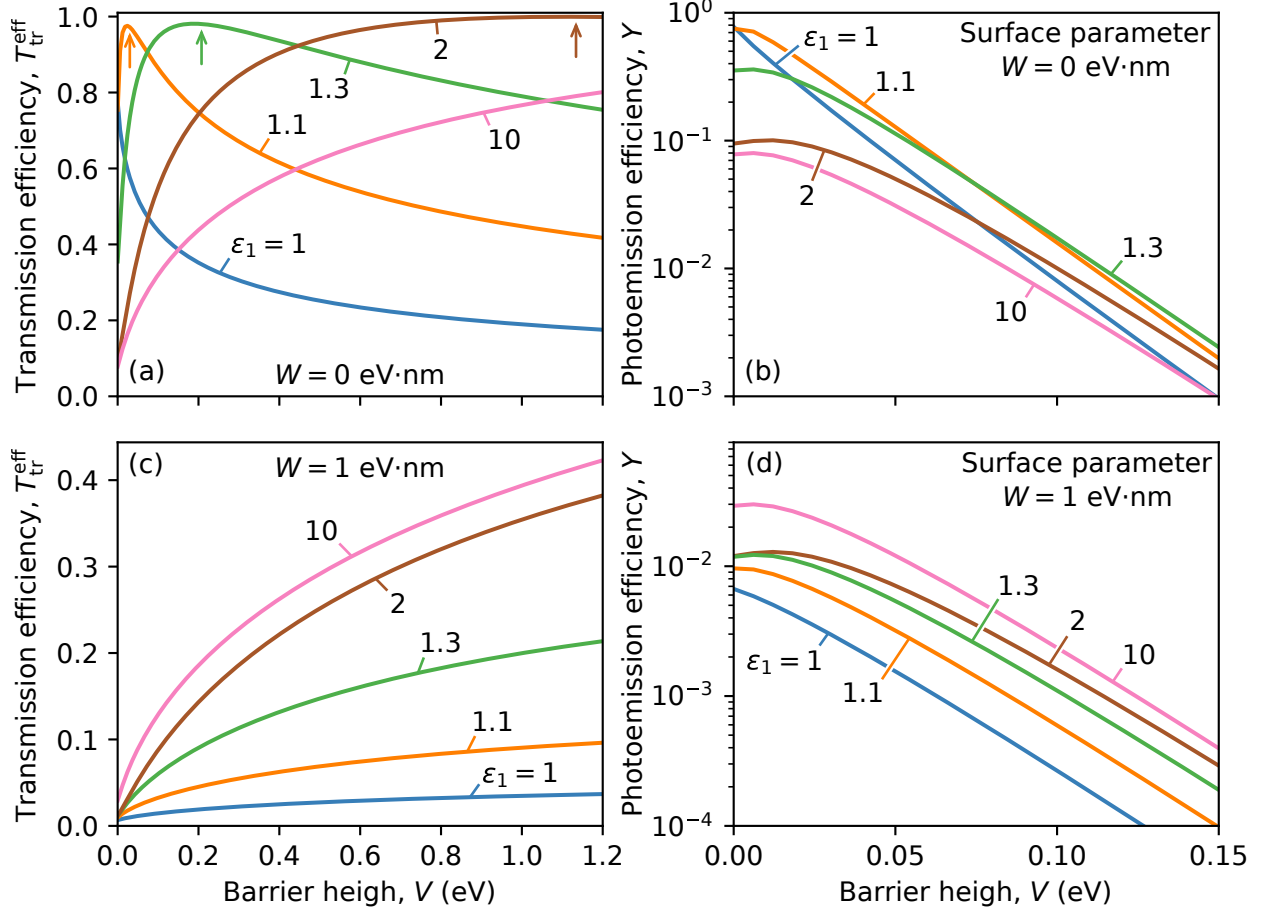


Figure 9. Dependencies of the transmission efficiency T_{tr}^{eff} (a, c) and photo-emission efficiency Y (b, d) on the barrier height V calculated for the surface parameter $W = 0$ (a, b) and for $W = 1 \text{ eV}\cdot\text{nm}$ (c, d) with different values of the dielectric constant ϵ_1 , and for $\epsilon_2 = 1$. Arrows in (a) show the values of the “optimal” barrier height V_{tr} from Eq. (49).

[27, 28] as the ratio of the emitted electron flux, taking into account the transmission coefficient T , to the total flux of electrons incident on the surface from the semiconductor volume. Considering only the normal incidence of electrons on the semiconductor/vacuum interface, we obtain

$$Y(W, V) = \frac{\int_0^\infty T_{tr}(W, E) k_1(E) e^{-E/k_B T} dk_1}{\int_0^\infty k_1(E) e^{-E/k_B T} dk_1}. \quad (57)$$

Here we assume that electrons are thermalized, and that their thermal-population is described by the Boltzmann distribution $f_B(E) = \exp(-E/k_B T)$, where $E = \hbar^2 k_1^2 / 2m_1$ is the electron energy, and k_B is the Boltzmann constant. One can see that in our one-dimensional

model the quantum efficiency of the photoemission can be expressed as follows:

$$Y(W, V) = \exp\left\{-\frac{V}{k_B T}\right\} T_{\text{tr}}^{\text{eff}}(W), \quad T_{\text{tr}}^{\text{eff}}(W) = \frac{\int_V^\infty T_{\text{tr}}(W, E) e^{-E/k_B T} dE}{\int_V^\infty e^{-E/k_B T} dE}. \quad (58)$$

Here $T_{\text{tr}}^{\text{eff}}(W)$ is the transmission efficiency. The dependence of $T_{\text{tr}}^{\text{eff}}(W)$ on the surface parameter W for $\varepsilon_2 = 1$, various values of ε_1 , and the barrier heights $V = 1$ eV and $V = 0.2$ eV is shown in Fig. 5(b) and Fig. 5(d), respectively. One can see that $T_{\text{tr}}^{\text{eff}}(W)$, and consequently $Y(V, W)$, significantly reduces with increase of $|W|$. The maximum of $T_{\text{tr}}^{\text{eff}}$ for a given value of ε_1 is reached at the non-zero (but usually small) value $W = W_{\text{tr}}$. Interestingly, for a fixed value of the surface parameter W and for $V > 0.18$ eV, the value $T_{\text{tr}}^{\text{eff}}$ taking into account the self-interaction potential U_{self} ($\varepsilon_1 > \varepsilon_2$) is larger than that for $q_1, q_2 = 0$.

Figure 9 shows the dependencies of the transmission efficiency $T_{\text{tr}}^{\text{eff}}(W)$ (a, c) and photoemission efficiency $Y(W, V)$ (b, d) on the barrier height V calculated for $W = 0$ (a, b) and $W = 1$ eV·nm (c, d) with $\varepsilon_2 = 1$ and various values of ε_1 . Unexpected non-monotonic dependence of $T_{\text{tr}}^{\text{eff}}(W)$ on V for $W = 0$ can be observed close to the optimal conditions. Figure 9 shows also that for $W = 1$ eV·nm (that is, far from the resonant condition) $T_{\text{tr}}^{\text{eff}}(W)$ unexpectedly increases with increase of V . Both these phenomena result from the perfect transmission conditions predicted by our theory. For $Y(V)$, the main tendency is the decrease of Y with the increase of V because of the exponential factor in the Boltzmann distribution. However, one can see that taking into account of the potential U_{self} gives rise to a non-monotonic dependence of Y on V for small values of V . Depending on the barrier height V and the value of the surface parameter W , an additional scattering on the mirror force potential U_{self} may increase or decrease the quantum efficiency of the photoemission.

B. Discrete spectrum of electrons in a surface quantum well

Next, we consider a quantum well (QW) between an infinite potential barrier at $z = -a$ and the discontinuity of the dielectric constant at $z = 0$. We focus our attention on the discrete spectrum of energy levels with $E < V$.

In the absence of dielectric discontinuity (the case of $q_1, q_2 = 0$), the discrete spectrum E_n^W is given by solutions of the equation:

$$\left(1 + \frac{2W}{\hbar^2} \frac{m_2}{\varkappa_2}\right) \tan(k_1 a) + \frac{k_1}{\varkappa_2} \frac{m_2}{m_1} = 0. \quad (59)$$

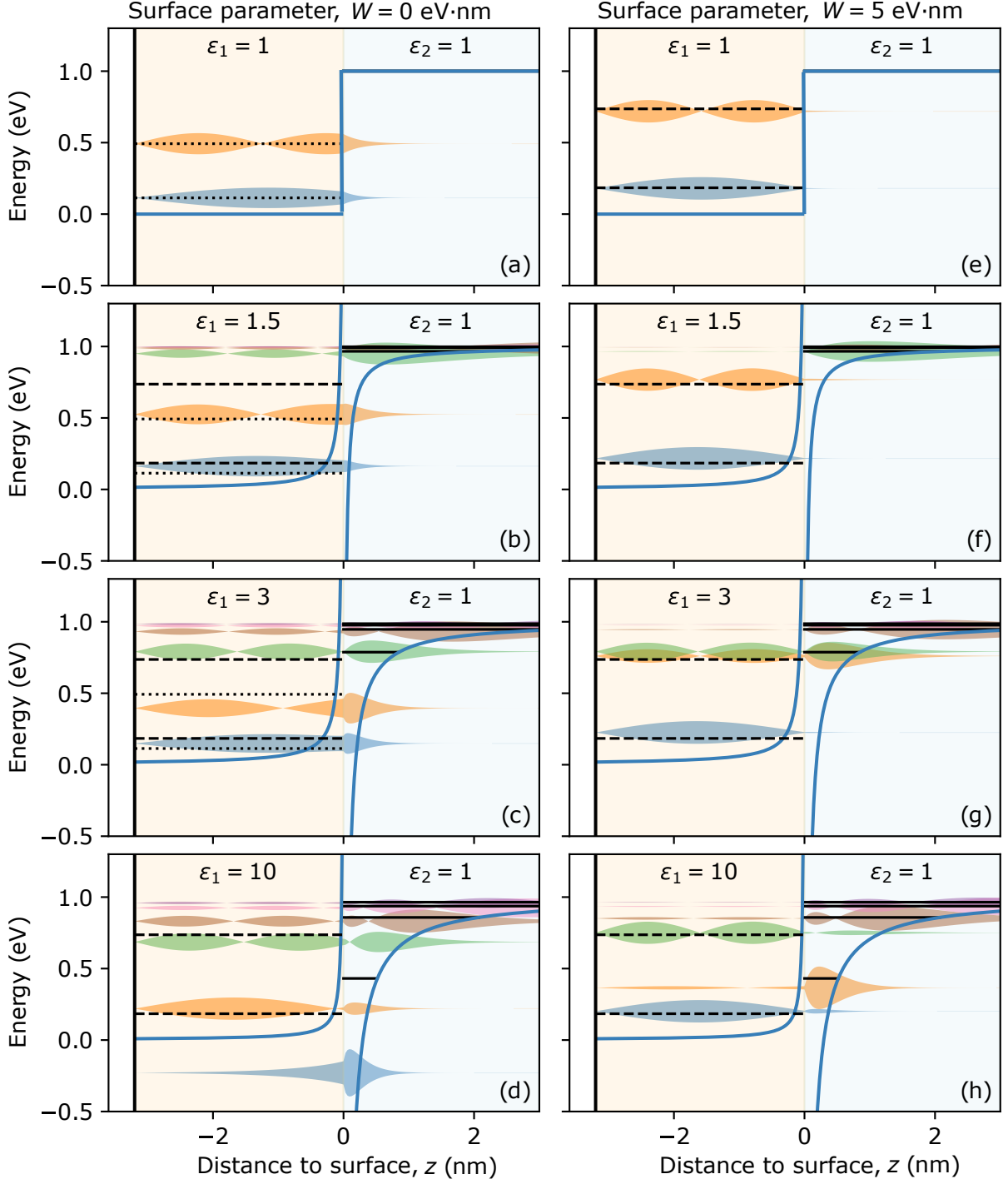


Figure 10. Electron states in the asymmetric quantum well calculated for various dielectric constants ε_1 . Horizontal solid lines show the energy levels E_n localized in the mirror force attractive potential; dashed lines — levels E_n^∞ in the QW with infinite barriers; dotted lines — levels E_n^0 in the asymmetric QW for $q_1, q_2 = 0$. Filled areas show the electron wave functions at the energy levels.

For $|W| \rightarrow \infty$, we obtain $E_n^W \rightarrow E_n^\infty$, where

$$E_n^\infty = \frac{\hbar^2 \pi^2 n^2}{2m_1 a^2}, \quad n = 1, 2, 3, \dots$$

are the energy levels in the symmetric QW with two infinite potential barriers. In this case, the surface parameter W can be directly interpreted as the power of the δ -function potential at $z = 0$ preventing electron tunneling.

In the absence of dielectric discontinuity and for $W = 0$, the number ν of confined levels, E_n^0 with $n = 1, 2, \dots, \nu$, localized in the asymmetric quantum well with a finite value of the band offset potential V , can be estimated by the condition

$$a\sqrt{2m_1 V} \geq \hbar\pi(\nu - 1/2), \quad (60)$$

where a is the quantum well width. Selecting a quantum well containing two quantum confined levels with energies E_1^0 and E_2^0 in the case of $q_1, q_2, W = 0$, and using the following material parameters: $m_1 = 0.2m_0$, $V = 1$ eV and $a = 3.2$ nm, we will investigate the effect of dielectric confinement and of the surface parameter W on the electron level structure.

In Figure 10, we show the electron energy spectrum and the profile of wave functions for such a well taking into account the mirror potential U_{self} for various values of $\varepsilon_1 = 1$ (a, e), 1.5 (b, f), 3 (c, g) and 10 (d, h). The values of the surface parameters are $W = 0$ eV·nm in the panels (a, b, c, d) and $W = 5$ eV·nm in the panels (e, f, g, h). Horizontal solid lines show the energies $E_n = V - \mathcal{R}_2/n^2$ (see Eq. (31)) given by the poles of the function $\Sigma(E)$ and being the levels created by mirror force potential attracting electron to the surface in the case of Dirichlet boundary conditions. Horizontal dashed lines show the energy levels E_n^∞ in the symmetric QW with infinite barriers at $z = -a$ and $z = 0$ for $q_1, q_2 = 0$. Horizontal dotted lines show the energy levels E_n^0 in the asymmetric QW with finite potential barrier $V = 1$ eV at $z = 0$ for $q_1, q_2, W = 0$. Filled areas show the profiles of electron wave functions corresponding to the localized states.

Comparing the panels (a) and (e), one can observe that for $q_1, q_2 = 0$ the boundary conditions with $W = 5$ eV·nm shift two electron energy levels in the QW from E_n^0 to E_n^∞ , and that the electron tunneling under the barrier is very weak. Even a small dielectric confinement (panels (b) and (f)) modifies the energy structure: resonant levels near the barrier appear with electron wave functions mostly localized in the dielectric area. With increase of the dielectric confinement, the levels with electrons localized both in the QW and in the dielectric appear including a surface localized state with $E < 0$ (see panel (d)).

Figure 11 shows the dependence of electron energy levels (blue lines) on the surface parameter W for various values of ε_1 . Horizontal dashed lines show energy levels E_n^∞ in the symmetric QW, orange lines – energy levels $E_n = V - \mathcal{R}_2/n^2$. One can see that even without dielectric confinement for $\varepsilon_1 = \varepsilon_2 = 1$ (Fig. 11(a)) the energy levels E_n^W in a QW can be dramatically modified by the presence of the surface short-range potential $W\delta(z)$. The dielectric confinement with $\varepsilon_1 > \varepsilon_2$ (Fig. 11(b, c, d)) has an additional effect of mixing the E_n^W QW states with the E_n states in the attractive potential $U_{\text{self}}(z)$.

Figure 12 shows the dependence of electron energy levels on the value of ε_1 for various values of the surface parameter W . The energy levels in the quantum well are shown by blue lines, while the orange lines show the energies $E_n = V - \mathcal{R}_2/n^2$. Horizontal dashed lines show energy levels E_n^∞ . As discussed above, the case of $W \rightarrow \pm\infty$ (Fig. 12(a)) corresponds to the Dirichlet boundary conditions $\psi_1(0) = \psi_2(0) = 0$. Correspondingly, the two electron states $E_{n=1,2}^{\text{QW}}$ are fully localized in the QW while the E_n states are localized in the attractive potential $U_{\text{self}}(z)$ in the dielectric. The dielectric confinement with $\varepsilon_1 \neq \varepsilon_2$ weakly affects the energies $E_{n=1,2}^{\text{QW}} \approx E_{n=1,2}^\infty$ by shifting them up. However, for the finite values of W allowing the electron tunneling under the barrier, the resulting energy states are superposition states of the electron in the quantum well and in the attractive potential $U_{\text{self}}(z)$ in the dielectric. It is worth noting that in this case the dramatic modification of the energy spectrum takes place already for $\varepsilon_1 < 2$, and that the potential $U_{\text{self}}(z)$ cannot be considered as a perturbation.

VI. DISCUSSION AND CONCLUSION

In this paper, we have presented a non-perturbative macroscopic theory for flat interfaces with a dielectric discontinuity. It gives rise to a self-consistent quantitative description of the leakage of the carrier wave function in the surrounding matrix, and such a description is crucial for the study of transport in nanocrystal arrays and solids. This theory also predicts several novel phenomena. The first one is the existence of perfect transmission conditions above the barrier, and of resonance levels with finite life time below the barrier that could potentially enhance photo-effect in some heterostructures. For surface quantum wells, it predicts strong coupling between internal confined levels and surface levels created by the attractive mirror potential for some interfaces. As a consequence, conductivity of an array of such structures should be enhanced. Furthermore, in addition to engineering of the potential

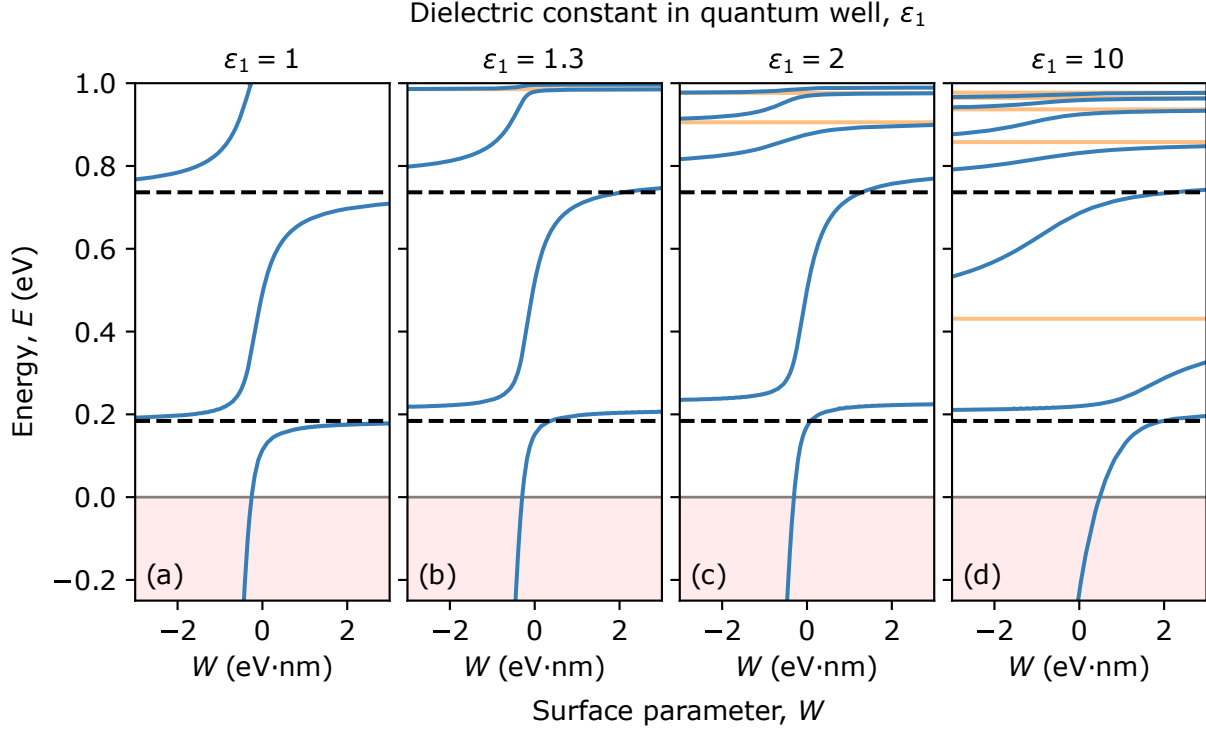


Figure 11. Dependence of the electron energy levels in the asymmetric quantum well on the surface parameter W calculated for dielectric $\varepsilon_2 = 1$ and dielectric constants $\varepsilon_1 = 1, 1.3, 2, 10$ in panel (a) to (d), respectively. The levels are shown by a blue lines. Horizontal dashed lines show the energy levels $E_{n=1,2}^\infty$ in the symmetric QW with infinite barriers for $q_1, q_2 = 0$, orange solid lines show the pole energies E_n for levels localized in the attractive potential of mirror force outside of semiconductor.

barrier, engineering of the dielectric discontinuity provides a new tool controlling transitions between bound states localized in quantum wells and resonance in the continuous spectrum [37].

The one-dimensional non-perturbative theory developed in this paper is only the first step in a self-consistent quantitative description of electronic and optical properties of nanostructures with dielectric discontinuities. The natural next step is to apply such a theory to nanostructures with high enough symmetry that would allow for an exact analytic expression for the mirror potential, and for a separation of variables in the corresponding Schrödinger equation. These include spherical and ellipsoidal nanocrystals, nanorods, nanowires, and nanoplatelets. In such structures, the non-perturbative theory is expected to provide a complete realistic description of quantum confined levels, of the oscillator transition strength of

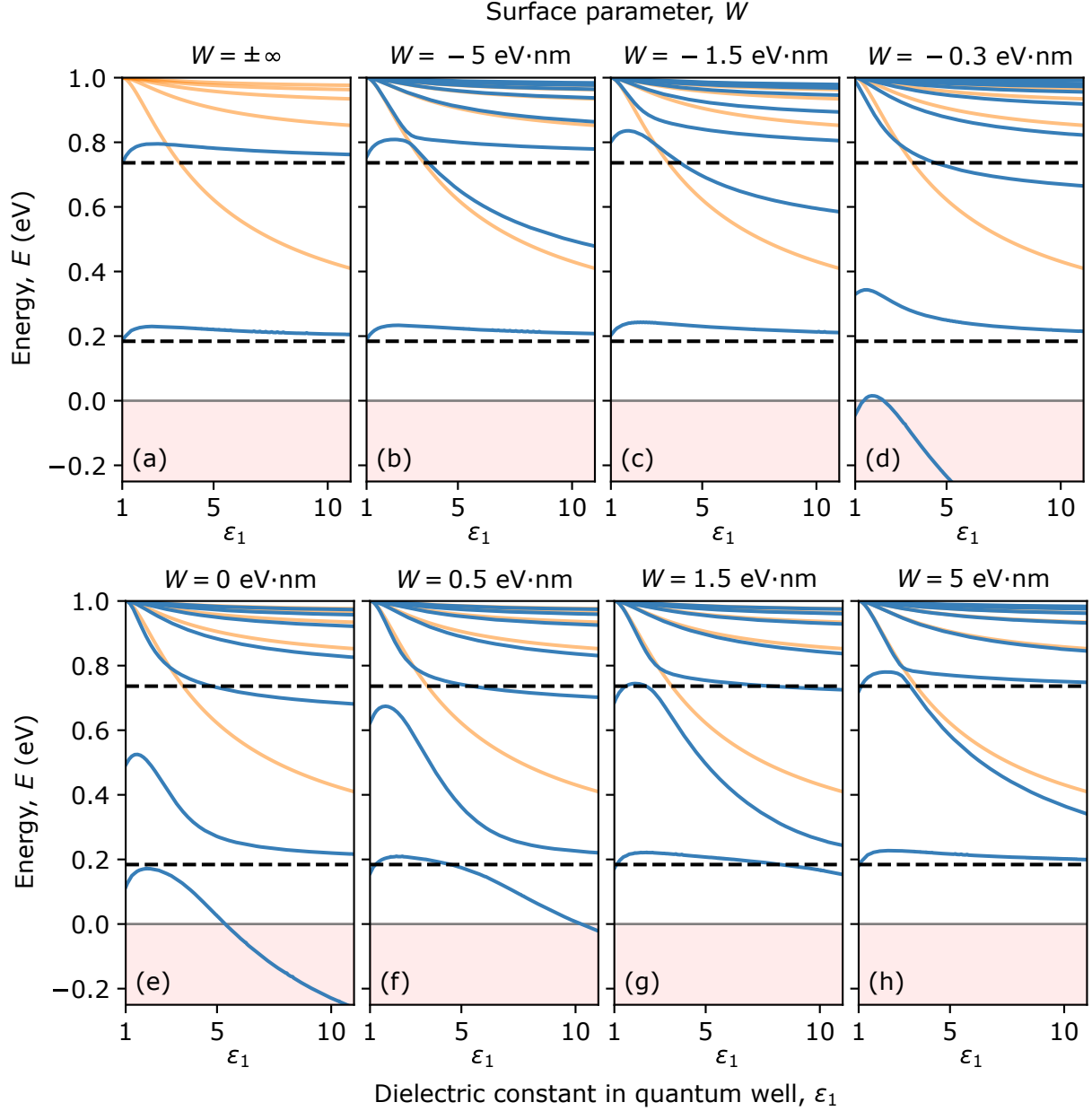


Figure 12. Dependence of the electron energy levels shown by blues lines in the asymmetric quantum well as a function of the dielectric constant $\epsilon = 1$, calculated for $\epsilon_2 = 1$ and surface parameter $W = \pm\infty$ and $W = -5, -1.5, -0.3, 0, 0.5, 1.5, 5$ eV·nm in panels (a) to (h), respectively. Orange lines show the pole energies E_n for levels localized in the attractive potential of mirror force outside of semiconductor. Horizontal dashed lines show the energy levels $E_{n=1,2}^\infty$ in the symmetric QW with infinite barriers for $q_1, q_2 = 0$.

the optical transition, of the electron-hole exchange interaction, *etc.* More ambitiously, the GBC of the type derived in this paper for interfaces with discontinuity of dielectric constants

should allow for a qualitative numerical description of all nanostructures.

ACKNOWLEDGMENTS

We are indebted to L. Parnovski for pointing out the reference [35], for the detailed explanations of the results of that paper, and for many valuable suggestions. We are grateful to M. Dykman, J. Galkowski, N. A. Gippius, A. A. Golovatenko, J. Lyons, M. Swift, S. G. Tikhodeev, and C. White for inspiring discussions.

Y.M.B. acknowledges support provided by the Ioffe Institute program FFUG-2024-0037. Research of A.V.R. and A.A. was supported in part by the grants 208235, 220040, and 236683, and by the National Center for Competence in Research (NCCR) SwissMAP of the Swiss National Science Foundation. A.A. acknowledges support of the award of the Simons Foundation to the Hamilton Mathematics Institute of the Trinity College Dublin under the program “Targeted Grants to Institutes”. Al.L.E acknowledges support by the Office of Naval Research through the Naval Research Laboratory’s Basic Research Program.

DATA AVAILABILITY STATEMENT

The data that support the findings of this study are available from the corresponding author upon reasonable request.

-
- [1] Al. L. Efros and A. L. Efros, “Interband absorption of light in semiconductor sphere”, *Sov. Phys. Semicond.* **16**, 772 (1982).
 - [2] L. E. Brus, “A simple model for the ionization potential, electron affinity, and aqueous redox potentials of small semiconductor crystallites”, *J. Chem. Phys.* **79**, 5566 (1983). doi: <https://doi.org/10.1063/1.445676>
 - [3] A. I. Ekimov, F. Hache, M. C. Shanne-Klein, D. Ricard, Ch. Flitzanis, I. A. Kudriavtsev, A. V. Rodina, and Al. L. Efros, “Absorption and intensity-dependent photoluminescence measurements on CdSe quantum dots: assignment of the first electronic transitions”, *Journal of the Optical Society of America B* **10**, 100 (1993). doi:10.1364/JOSAB.10.000100

- [4] Al. L. Efros and M. Rosen, “Quantum size level structure of narrow-gap semiconductor nanocrystals: effect of band coupling”, *Phys. Rev. B* **58**, 7120 (1998). doi: <https://doi.org/10.1103/PhysRevB.58.7120>
- [5] Al. L. Efros and M. Rosen, “The electronic structure of semiconductor nanocrystals”, *Annual Review of Material Science* **30**, 455 (2000). doi: <https://doi.org/10.1146/annurev.matsci.30.1.475>
- [6] P. C. Sercel and K. J. Vahala, “Analytical formalism for determining quantum-wire and quantum-dot band structure in the multiband envelope-function approximation”, *Phys. Rev. B* **42**, 3690 (1990). doi:<https://doi.org/10.1103/PhysRevB.42.3690>
- [7] I. Kang and F. W. Wise, “Electronic structure and optical properties of PbS and PbSe quantum dots”, *Journal of the Optical Society of America B* **14**, 1632 (1997). doi: [10.1364/JOSAB.14.001632](https://doi.org/10.1364/JOSAB.14.001632)
- [8] M. A. Becker, R. Vaxenburg, G. Nedelcu, P. C. Sercel, A. Shabaev, M. J. Mehl, J. G. Michopoulos, S. G. Lambrakos, N. Bernstein, J. L. Lyons, T. Stöferle, R. F. Mahrt, M. V. Kovalenko, D. J. Norris, G. Rainò, and Al. L. Efros, “Bright triplet excitons in caesium lead halide perovskites”, *Nature* **553**, 189 (2018). doi:<https://doi.org/10.1038/nature25147>
- [9] A. Shabaev and Al. L. Efros, “One-dimensional exciton spectroscopy in semiconductor nanorods”, *Nano Lett.* **4**, 1821 (2004). doi:<https://doi.org/10.1021/nl049216f>
- [10] S. Ithurria, M. D. Tessier, B. Mahler, R. P. S. M. Lobo, B. Dubertret, and Al. L. Efros, “Colloidal nanoplatelets with two-dimensional electronic structure”, *Nature Materials* **10**, 936 (2011). doi:<https://doi.org/10.1038/nmat3145>
- [11] L.-W. Wang and A. Zunger, “Pseudopotential-based multiband $\mathbf{k} \cdot \mathbf{p}$ method for $\sim 250\,000$ -atom nanostructure systems”, *Phys. Rev. B* **54**, 11417 (1996). doi: <https://doi.org/10.1103/PhysRevB.54.11417>
- [12] A. Puzder, A. J. Williamson, F. Gygi, and G. Galli, “Self-Healing of CdSe Nanocrystals: First-Principles Calculation”, *Phys. Rev. Lett.* **92**, 217401 (2004). doi: <https://doi.org/10.1103/PhysRevLett.92.217401>
- [13] M. Korkusinski, O. Voznyy, and P. Hawrylak, “Fine structure and size dependence of exciton and biexciton optical spectra in CdSe nanocrystals”, *Phys. Rev. B* **82**, 245304 (2010). doi: <https://doi.org/10.1103/PhysRevB.82.245304>

- [14] S. Küfner, J. Furthmüller, L. Matthes, M. Fitzner, and F. Bechstedt, “Structural and electronic properties of α -tin nanocrystals from first principles”, Phys. Rev. B **87**, 235307 (2013). doi:<https://doi.org/10.1103/PhysRevB.87.235307>
- [15] A. Franceschetti, “Structural and electronic properties of PbSe nanocrystals from first principles”, Phys. Rev. B **78**, 075418 (2008). doi:<https://doi.org/10.1103/PhysRevB.78.075418>
- [16] T. Ando and S. Mori, “Effective-mass theory of semiconductor heterojunctions and superlattices”, Surface Science **113**, 124 (1982). doi:[10.1016/0039-6028\(82\)90572-6](https://doi.org/10.1016/0039-6028(82)90572-6)
- [17] Q. G. Zhu and H. Kroemer, “Interface connection rules for effective-mass wave functions at an abrupt heterojunction between two different semiconductors”, Phys. Rev. B **27**, 3519 (1983). doi:[10.1103/PhysRevB.27.3519](https://doi.org/10.1103/PhysRevB.27.3519)
- [18] T. Ando, S. Wakahara, and H. Akera, “Connection of envelope functions at semiconductor heterointerfaces. I. Interface matrix calculated in simplest models”, Phys. Rev. B **40**, 11609, (1989). doi:<https://doi.org/10.1103/PhysRevB.40.11609>
- [19] A. V. Rodina, A. Yu. Alekseev, Al. L. Efros, M. Rosen, and B. K. Meyer, “General boundary conditions for the envelope function in the multiband $\mathbf{k} \cdot \mathbf{p}$ model”, Phys. Rev. B **65**, 125302 (2002). doi:[10.1103/PhysRevB.65.125302](https://doi.org/10.1103/PhysRevB.65.125302)
- [20] A. V. Rodina, A. L. Efros, and A. Y. Alekseev, “Effect of the surface on the electron quantum size levels and electron g factor in spherical semiconductor nanocrystals”, Phys. Rev. B **67**, 155312 (2003). doi:[10.1103/PhysRevB.67.155312](https://doi.org/10.1103/PhysRevB.67.155312)
- [21] A. V. Rodina and A. Y. Alekseev, “Least-action principle for envelope functions in abrupt heterostructures”, Phys. Rev. B **73**, 115312 (2006). doi:[10.1103/PhysRevB.73.115312](https://doi.org/10.1103/PhysRevB.73.115312)
- [22] L. D. Landau and E. M. Lifshitz, *Course of Theoretical Physics, Vol. 8: Electrodynamics of Continuous Media* (Pergamon, Oxford, 1960).
- [23] B. Ji, E. Rabani, Al. L. Efros, R. Vaxenburg, O. Ashkenazi, D. Azulay, U. Banin, and O. Millo, “Dielectric Confinement and Excitonic Effects in Two-Dimensional Nanoplatelets”, ACS Nano **14**, 8257 (2020). doi:[10.1021/acsnano.0c01950](https://doi.org/10.1021/acsnano.0c01950)
- [24] M. Dykman, private communication.
- [25] A. R. Khabibullin, Al. L. Efros, and S. C. Erwin, “The role of ligands in electron transport in nanocrystal solids”, Nanoscale **12**, 23028 (2020). doi:<https://doi.org/10.1039/D0NR06892F>
- [26] S. C. Erwin and Al. L. Efros, “Electronic transport in quantum-dot-in-perovskite solids”, Nanoscale **14**, 17725 (2022). doi: <https://doi.org/10.1039/D2NR04244D>

- [27] V. L. Alperovich, D. M. Kazantsev, A. G. Zhuravlev, and L. D. Shvartsman, “Photoemission and Photon-Enhanced Thermionic Emission: Effect of Jump in Electron Mass”, *Applied Surface Science* **561**, 149987 (2021). doi:10.1016/j.apsusc.2021.149987.
- [28] D.M. Kazantsev, V.S. Khoroshilov, H.E. Scheibler, and V.L. Alperovich, “Electron transfer through semiconductor-vacuum interfaces with negative and positive electron affinity: effect of jump in mass”, *Physics of the Solid State* **65**, 1219 (2023). doi:10.61011/PSS.2023.08.56565.130
- [29] E. A. Muljarov, S. G. Tikhodeev, and T. Ishihara, “Dielectrically confined excitons in natural superlattices -perovskite lead iodite semiconductors”, *Proc. SPIE* **1985**, 784 (1993). doi:10.1117/12.162738
- [30] E. A. Muljarov, S. G. Tikhodeev, N. A. Gippius, and T. Ishihara, “Excitons in self-organized semiconductor/insulator superlattices: PbI-based perovskite compounds”, *Phys. Rev. B* **51**, 14370 (1995). doi:10.1103/PhysRevB.51.14370
- [31] L.V. Kulik, V. D. Kulakovskii, M. Bayer, A. Forchel, N. A. Gippius, and S. G. Tikhodeev, “Dielectric enhancement of excitons in near-surface quantum wells”, *Phys. Rev. B* **54**, R2335 (1996). doi:10.1103/PhysRevB.54.R2335
- [32] M. Kumagai and T. Takagahara, “Excitonic and nonlinear-optical properties of dielectric quantum-well structures”, *Phys. Rev. B* **40** 12359 (1989). doi:10.1103/PhysRevB.40.12359
- [33] F. Stern, “Image potential near a gradual interface between two dielectrics”, *Phys. Rev B* **17**, 5009 (1978). doi:https://doi.org/10.1103/PhysRevB.17.5009
- [34] C. R. de Oliveira and A. A. Verri, “Self-adjoint extensions of Coulomb systems in 1, 2 and 3 dimensions”, *Annals of Physics*, **324**, 251 (2009). doi:https://doi.org/10.1016/j.aop.2008.06.001
- [35] Y. Golovaty, “1D Schrödinger operators with Coulomb-like potentials”, *Journal of Mathematical Physics* **60**, 082105, (2019). doi:10.1063/1.5099309
- [36] R. A. Morrow and K. R. Brownstein, “Model effective-mass Hamiltonians for abrupt heterojunctions and the associated wave-function-matching conditions”, *Phys. Rev. B* **30**, 678 (1984). doi:https://doi.org/10.1103/PhysRevB.30.678
- [37] Y. Huang and S. Das Sarma, “Bound state continuum resonance transition in a shallow quantum well”, *Phys. Rev. B* **110**, 155425 (2024). doi:10.1103/PhysRevB.110.155425